Stem cell-released oncolytic herpes simplex virus has therapeutic efficacy in brain metastatic melanomas

Wanlu Du[a], Ivan Seah[a], Oumaima Bougazzoul[a], GiHun Choi[a,b], Katrina Meeth[c], Marcus W. Bosenberg[c,d], Hiroaki Wakimoto[a,b,e], David Fisher[f], and Khalid Shah[a,b,g,h,1]

[a]Center for Stem Cell Therapeutics and Imaging, Department of Radiology, Massachusetts General Hospital, Harvard Medical School, Boston, MA 02114; [b]Center for Stem Cell Therapeutics and Imaging Department of Neurosurgery, Brigham and Women's Hospital, Harvard Medical School, Boston, MA 02115; [c]Department of Pathology, Yale School of Medicine, New Haven, CT 06520; [d]Department of Dermatology, Yale School of Medicine, New Haven, CT 06520; [e]Department of Neurosurgery, Massachusetts General Hospital, Harvard Medical School, Boston, MA 02114; [f]Department of Dermatology, Massachusetts General Hospital, Harvard Medical School, Boston, MA 02114; [g]Department of Neurology, Massachusetts General Hospital, Harvard Medical School, Boston, MA 02114; and [h]Harvard Stem Cell Institute, Harvard University, Cambridge, MA 02138

Edited by Patrick S. Moore, University of Pittsburgh Cancer Institute, Pittsburgh, PA, and approved June 8, 2017 (received for review January 8, 2017)

The recent Food and Drug Administration approval of immunogenic oncolytic virus (OV) has opened a new era in the treatment of advanced melanoma; however, approximately 50% of patients with melanoma develop brain metastasis, and currently there are no beneficial treatment options for such patients. To model the progression of metastases seen in patients and to overcome the hurdles of systemic delivery of OV, we developed melanoma brain metastasis models in immunocompromised and immunocompetent mice, and tested the fate and efficacy of oncolytic herpes simplex virus (oHSV)-armed mesenchymal stem cells (MSCs). Using brain-seeking patient-derived melanoma cells and real-time in vivo imaging, we show a widespread distribution of micrometastases and macrometastases in the brain, recapitulating the progression of multifoci metastases seen in patients. We armed MSCs with different oHSV variants (MSC-oHSV) and found that intracarotid administration of MSC-oHSV, but not of purified oHSV alone, effectively tracks metastatic tumor lesions and significantly prolongs the survival of brain tumor-bearing mice. In a syngeneic model of melanoma brain metastasis, a combination of MSC-oHSV and PD-L1 blockade increases IFNγ-producing $CD8^+$ tumor-infiltrating T lymphocytes and results in a profound extension of the median survival of treated animals. This study thus demonstrates the utility of MSCs as OV carriers to disseminated brain lesions, and provides a clinically applicable therapeutic platform to target melanoma brain metastasis.

stem cells | oncolytic virus | tumors | metastasis | imaging

Melanoma, the most aggressive type of skin cancer, accounts for a large proportion of skin cancer-related deaths (1). Among all cancer types, melanoma has a particularly high propensity to metastasize to the brain, occurring in >50% of all patients with advanced disease. More than 90% of melanoma brain metastases lead to death, and the median survival is 17–22 wk after detection (2–4).

Current therapeutic options of chemotherapy, surgery, and radiation have very limited efficacy for patients with melanoma brain metastasis (5–7). These patients either have multiple metastatic lesions or diagnostically challenging asymptomatic lesions, making surgery an inadequate therapeutic option by itself. In addition, the blood-brain barrier (BBB) limits central nervous system (CNS) penetration of systemic therapies, and the negative side effects of radiotherapy (8) pose challenges for the success of existing therapies, contributing to the failure to improve overall patient survival. As such, there is an urgent need for new therapies for melanoma brain metastasis.

The development and characterization of preclinical tumor models that authentically recapitulate the clinical disease settings are critical for developing and testing new therapies. Most previous studies have used either subcutaneous (s.c.) injection or intracranial injection of established melanoma lines in mice (9–11), which do not mimic the actual clinical settings of melanoma brain metastasis, such as initial adhesion of tumor cells to brain capillaries, extravasation, continuation of perivascular position, vessel co-option, micrometastatic growth, and macrometastatic growth (12). In addition, long-established melanoma lines often fail to recapitulate the key aspects of human malignancy and thus poorly predict the clinical efficacy of tested therapeutic agents (13).

In this study, we created in vivo imageable mouse models of melanoma brain metastasis by internal carotid artery (ICA) injection of patient-derived primary melanoma and brain-seeking melanoma lines [either *BRAF* mutant or wild type (WT)], as well as the syngeneic mouse model of melanoma brain metastasis using a *BRAF* mutant line isolated from $Braf^{V600E/wt}Cdkn2A^{-/-}Pten^{-/-}$ mice.

Oncolytic viruses (OVs) that selectively replicate in tumor cells are an emerging modality of cancer treatment that shows promising results in both preclinical studies and clinical trials (14, 15). Among these OVs, oncolytic herpes simplex viruses (oHSV) have shown promising therapeutic efficacy in treating advanced melanoma (16, 17). Recently, the US Food and Drug Administration approved talimogene laherparepvec (T-VEC) for the treatment of melanoma lesions in the skin and lymph nodes (17). Although induction of an antitumor immune response is implicated in activity for distant uninjected lesions, T-VEC has not been shown to improve overall patient survival of stage IVM1b and IVM1c disease that has metastatic lesions to the brain, bone, liver, lungs, or other internal organs (18). The unavailability of appropriate clinically translatable mouse models of melanoma brain metastasis and issues related to oHSV delivery via the bloodstream (19), such as virus neutralization, sequestration, and inefficient extravasation, pose major barriers to the development of oHSV-based therapies for melanoma brain metastasis.

Significance

This study provides an insight into stem cell-based oncolytic virus therapies for advanced melanoma tumors that have metastasized into the brain by developing clinically relevant mouse tumor models and testing the fate and efficacy of oncolytic herpes simplex virus-armed mesenchymal stem cells in such models. This study therefore overcomes the hurdles of systemic delivery of oncolytic viruses and provides a clinically applicable therapeutic platform to target melanoma brain metastasis.

Author contributions: W.D. and K.S. designed research; W.D., I.S., O.B., G.C., and H.W. performed research; W.D., K.M., M.W.B., H.W., and D.F. contributed new reagents/analytic tools; W.D., I.S., O.B., G.C., H.W., D.F., and K.S. analyzed data; and W.D., H.W., D.F., and K.S. wrote the paper.

Conflict of interest statement: K.S. owns equity in, and is a member of the Board of Directors of, AMASA Technologies.

This article is a PNAS Direct Submission.

[1]To whom correspondence should be addressed. Email: kshah@bwh.harvard.edu.

This article contains supporting information online at www.pnas.org/lookup/suppl/doi:10.1073/pnas.1700363114/-/DCSupplemental.

Previous studies from our laboratory demonstrated that therapeutic human and mouse stem cells home extensively to multiple tumor deposits in the brain (20) and act as cell carriers for onsite delivery of tumor-specific agents or OV (21) in mouse models of different brain tumor types (22). In the present study, we tested the therapeutic efficacy of MSC-loaded oHSV (MSC-oHSV) in both *BRAF* mutant and WT in vivo imageable mouse models of melanoma brain metastasis, and explored the combined therapeutic efficacy of PD-L1 blockade and MSC-oHSV in a syngeneic mouse model of melanoma brain metastasis.

Results

A Panel of Human Melanoma Lines Respond to oHSV. Considering both malignancy and mutational status (23), we chose both established malignant human melanoma lines (SK-Mel-2, SK-Mel-28, MALME-3M, and MeWo) and patient-derived brain metastatic melanoma lines (TXM-13, M12, and M15). We tested the efficacy of the G47Δ-based recombinant oHSV in which cDNA encoding the mCherry fluorescent protein is placed under the IE4/5 immediate-early promoter of HSV (oHSV-mCh) on these lines. Low-multiplicity of infection (MOI) oHSV-mCh infection led to rapid production and spread of oHSV in tumor cells over time (Fig. 1 *A* and *B*), which resulted in robust dose-dependent cell killing (Fig. 1*C*) in all tested cell lines but had no significant effect on the viability of normal nonproliferating human astrocyte cultures (*SI Appendix*, Fig. S1). In parallel, we tested the efficacy of promising clinically approved therapeutic agents for advanced melanoma patients. Cell viability assays revealed minor effects of BRAF inhibitor PLX4720 in *BRAF* mutant (SK-Mel-28, MALME-3M, and M12) melanoma lines and no effects in *BRAF* WT (SK-Mel-2, MeWo, TXM-13, and M15) lines (*SI Appendix*, Fig. S2*A*). Similarly, treatment with temozolomide (TMZ) and low-dose cisplatin showed marginal effects on melanoma cell viability (*SI Appendix*, Fig. S2 *B* and *C*). These results indicate the unique ability of oHSV to target a broad spectrum of malignant melanoma lines with a robust cell-killing effect regardless of their *BRAF* mutational status.

Development and Characterization of Melanoma Brain Metastasis Mouse Models. To establish in vivo melanoma brain metastasis mouse models that recapitulate the steps of metastatic progression seen in patients, we chose two human melanoma lines, MeWo (*BRAF* WT, pigmented), which was isolated from lymph nodes of a patient with advanced melanoma, and M12 (*BRAF* mutant, nonpigmented), which was directly isolated from a melanoma brain metastasis. Both cell lines were engineered to express a bimodal firefly luciferase (Fluc)-mCherry (FmC) protein (*SI Appendix*, Fig. S3 *A* and *B*). To mimic the critical steps of metastatic

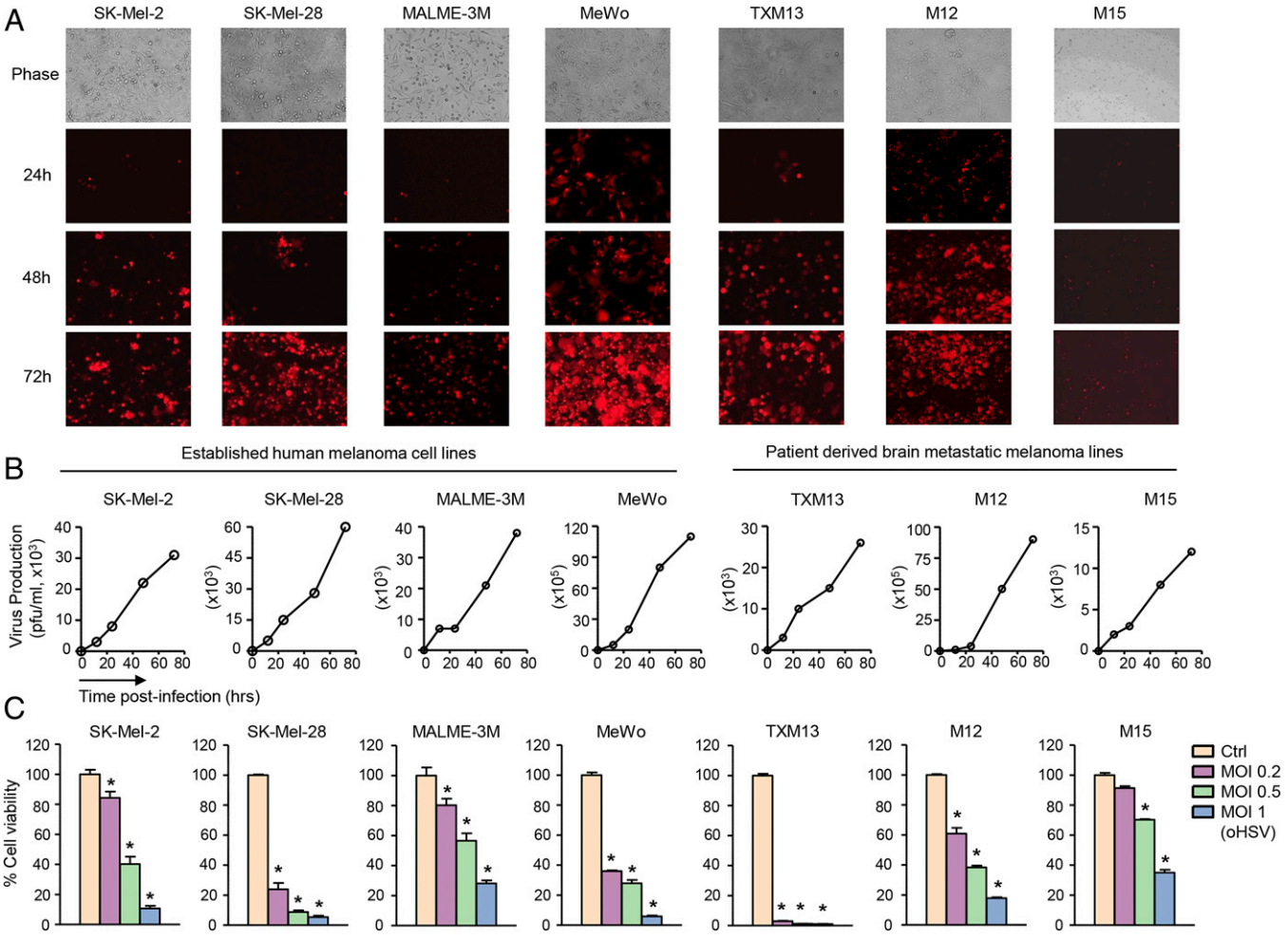

Fig. 1. oHSV replicates in human melanoma cells and kills them by viral oncolysis. (*A*) Four established human melanoma cell lines and three patient-derived brain metastatic melanoma cell lines were infected with oHSV-mCh at MOI of 0.2. Representative fluorescence microscopic images at different time points are shown. (Magnification: 10×) (*B*) Human melanoma cells were infected with oHSV, and the virus production postinfection was measured by a plaque assay. (*C*) Human melanoma cells were infected with oHSV at different MOI (0.2–1), and cell viability was analyzed at day 4 after virus infection. $^*P < 0.05$ vs. uninfected controls (Ctrl).

colonization and blood vessel interactions, MeWo-FmC and M12-FmC were injected via the ICA into immunocompromised mice (Fig. 2*A*). Noninvasive bioluminescence imaging (BLI) of tumor-bearing mice revealed brain metastasis and exponential growth of metastatic tumors in the brain at 2–3 wk post-ICA injection of tumor cells (Fig. 2 *B* and *C*). Pigmented metastatic foci were seen in the brains bearing MeWo-FmC tumors (Fig. 2*D*), whereas no pathological changes were apparent in the brains bearing M12-FmC tumors (Fig. 2*H*). However, at a cellular level, fluorescent images confirmed the presence of mCherry-positive (mCh^+) tumor cells within macrometastatic foci in both models (Fig. 2 *E* and *I*).

Further immunohistochemistry analysis of brain sections from tumor-bearing mice demonstrated that metastatic melanoma cells (mCh^+) were proliferative ($Ki67^+$) and associated with reactive astrocytes ($GFAP^+$) (MeWo-FmC, Fig. 2 *F* and *G*; M12-FmC, Fig. 2 *J* and *K*). Coronal brain sections from mice bearing M12-FmC brain metastases at different time points after tumor cell injection showed that tumor cells distributed across all representative sections and the number and size of metastases increased over time, consistent with increased bioluminescence (Fig. 2*L*). Quantitative assessment of mCherry fluorescence on brain sections along the anteroposterior axis at 14, 21, and 28 d post–M12-FmC cell implantation revealed distinct tumor foci that were detectable as early as 14 d, along with widespread distribution of micrometastases and macrometastases in the later stages of metastatic progression (days 21 and 28; Fig. 2*M*). Our results show that ICA injection of patient-derived malignant melanoma cells generates clinically relevant mouse models that resemble the development of multifoci melanoma brain metastases observed in the clinic.

MSCs Act as Cellular Vehicles for oHSV Delivery. To assess the survival and viral spread of human MSCs freshly loaded with oHSV-mCh (MSC-oHSV-mCh) in vitro, MSCs were infected with oHSV-mCh at different MOI. The increased expression of mCherry within MSCs over time indicated efficient spread and amplification of oHSV-mCh (*SI Appendix*, Fig. S4). Cell viability assays of MSCs loaded with oHSV at different MOI showed that ∼90% of MSC-oHSV survived at least 4 d postinfection with an MOI of 0.2 or 0.5, and >60% MSC-oHSV survived with an MOI of 1 (Fig. 3*A*).

In parallel, we tested whether human MSCs had any influence on the growth of melanoma cells in culture and in vivo. We first engineered MeWo cells to express GFP (MeWo-GFP) and combined GFP and Fluc markers (MeWo-GFP-Fluc). Fluc bioluminescent imaging revealed that MSC cocultured with MeWo-GFP-Fluc cells or ICA-injected into mice bearing MeWo-GFP-Fluc tumors did not result in any changes in tumor cell growth in vitro or in vivo (*SI Appendix*, Fig. S5).

To further assess the oncolytic activity of MSC-released oHSV-mCh on melanoma cells, we cocultured MeWo-GFP cells with MSC-oHSV-mCh. Dual fluorescent imaging revealed the release of oHSV-mCh from MSCs (representative as red cell population), which resulted in the infection of adjacent MeWo-GFP cells and spread of oHSV-mCh among melanoma cells

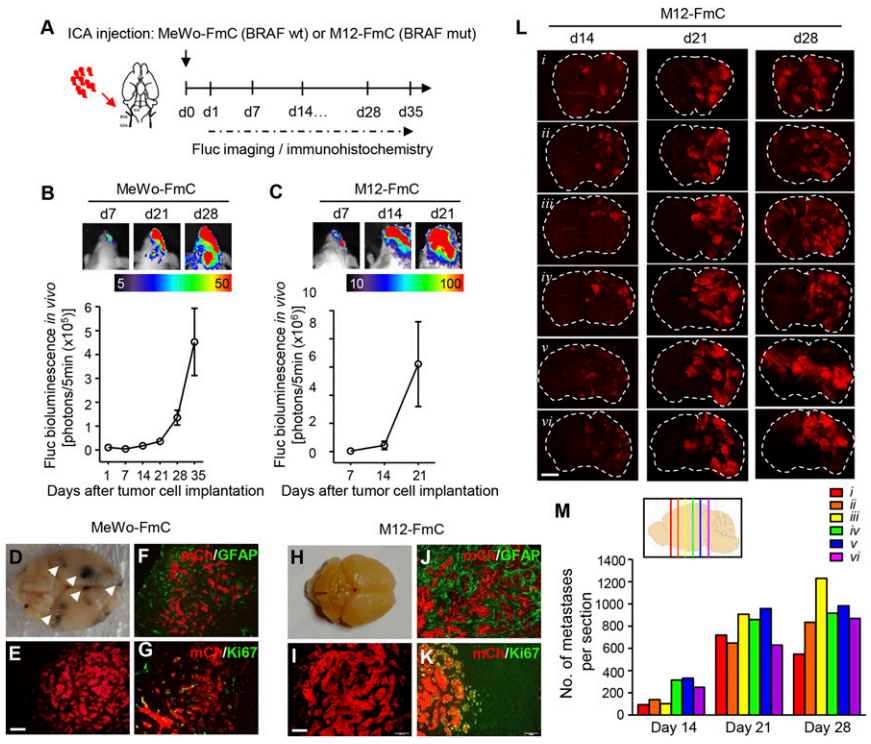

Fig. 2. Characterizing in vivo imageable melanoma brain metastasis mouse models. (*A*) Experimental outline showing tumor cell implantation and subsequent imaging/immunohistochemistry studies. Red arrow indicates the route of tumor cell injection. Black arrow indicates the time point of tumor cell implantation. (*B* and *C*) Representative bioluminescent images of MeWo-FmC (*B*) and M12-FmC (*C*) tumors after ICA injection of tumor cells (*Top*) and plot showing the in vivo tumor growth of MeWo-FmC or M12-FmC over time (*Bottom*); $n = 3$ mice per cell line. (*D* and *H*) Representative images showing multiple pigmented foci (white arrowheads) of MeWo-FmC ICA-injected mouse brain (*D*) and nonpigmented M12-FmC ICA-injected mouse brain (*H*). (*E* and *I*) Fluorescent images of metastatic foci in the brain: (*E*) MeWo-FmC; (*I*) M12-FmC. (*F*, *G*, *J*, and *K*) Representative fluorescent images of GFAP or Ki67 immunostaining (green) on brain sections showing proliferative metastatic melanoma cells ($Ki67^+$; mCh^+) surrounded by reactive astrocytes ($GFAP^+$). (*L*) Composite fluorescent images of coronal brain sections of mice bearing metastatic M12-FmC tumors from different planes along the anteroposterior axis (*i*–*vi*). (*M*) Quantification of micrometastatic and macrometastatic foci in the brain. (*Inset*) The location of each coronal section along the anteroposterior axis (*i*–*vi*). (Scale bars: *E* and *I*, 100 μm, also applies to *F*, *G*, *J*, and *K*; *L*, 2 mm.)

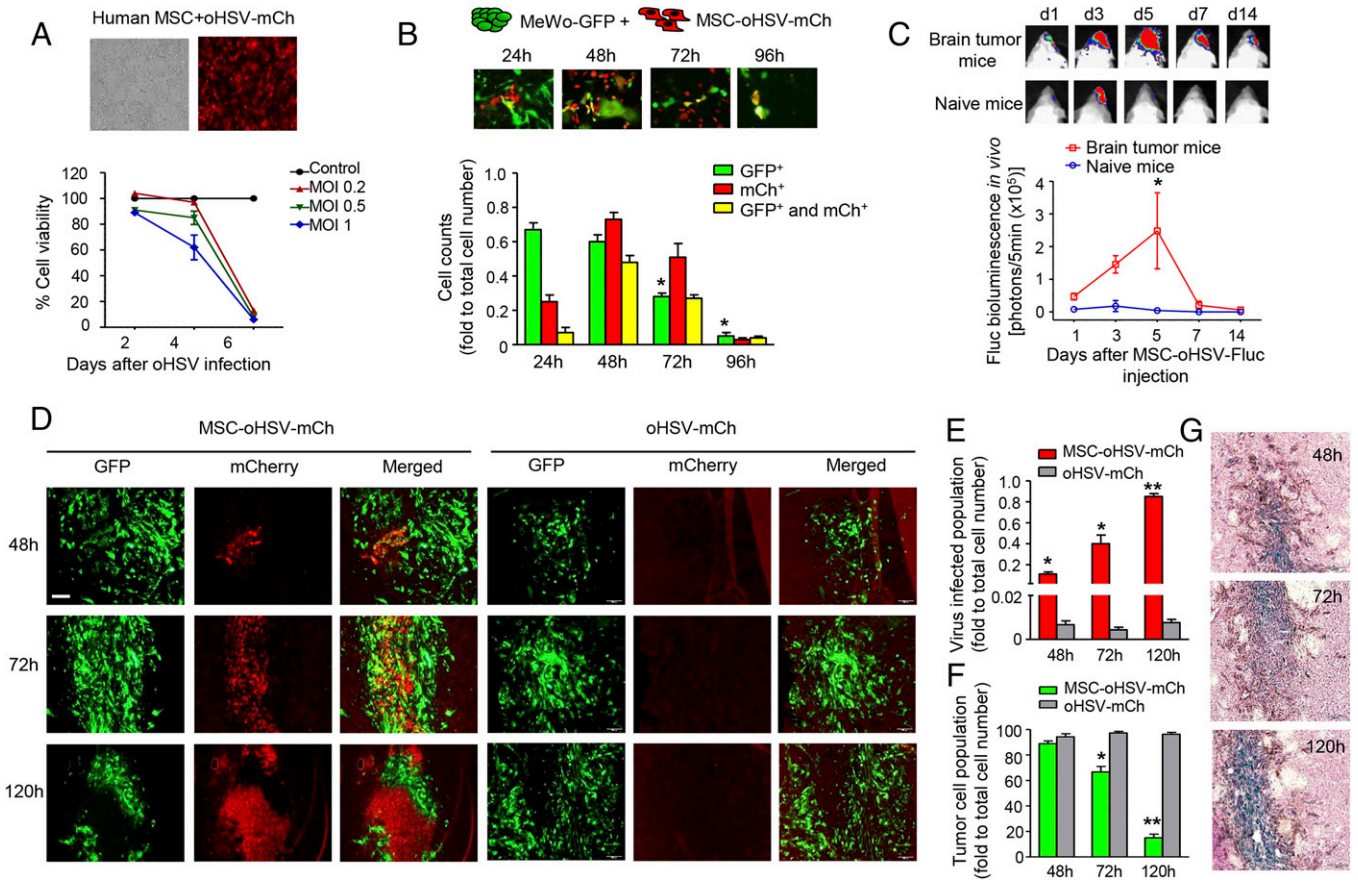

Fig. 3. In vivo imaging of MSC-mediated delivery of oHSV in mouse models of melanoma brain metastasis. (*A*) Cell viability of MSCs infected with oHSV-mCh at the indicated MOI analyzed at days 2, 4, and 6 postinfection. Representative phase and fluorescent images of human MSCs infected with oHSV-mCh at an MOI of 1 (24 h postinfection) are shown. (Magnification: 10×.) (*B*) MSC-oHSV-mCh were cocultured with MeWo-GFP at a 1:1 ratio, and populations of tumor cells (green), oHSV-mCh loaded MSCs (red), and oHSV-mCh–infected tumor cells (yellow) were analyzed at different time points. Representative fluorescent images show the coculture of MeWo-GFP and MSC-oHSV-mCh over time. (Magnification: 20×.) (*C*) Plot showing Fluc activity after MSC-oHSV-Fluc ICA injection in the melanoma metastatic brain tumor mice group and naive mice group. Representative bioluminescent images at different time points are shown. $*P < 0.05$ vs. naive mice ($n = 3$ mice per group). (*D*) Fluorescent images showing the population of tumor cells (GFP^+) and oHSV-mCh–infected cells (mCh^+) after ICA injection of MSC-oHSV-mCh or purified oHSV-mCh at the indicated time points. (Scale bar: 100 μm.) (*E* and *F*) Plots showing the populations of oHSV-mCh–infected cells (*E*) and tumor cells only (*F*) in the brain at different time points after ICA injection of MSC-oHSV-mCh or purified oHSV-mCh. $*P < 0.05$, $**P < 0.01$ vs. the oHSV-mCh–injected group ($n = 3$ mice per group). (*G*) Photomicrographs showing the time-dependent increase in $LacZ^+$-infected cells after ICA injection of MSC-oHSV-mCh. (Magnification: 10×.)

(representative as yellow cell population), leading to extensive oncolysis and a significant decrease in tumor cell number (green cell population) (Fig. 3*B*).

To visualize the activity and dynamics of oHSV delivered by MSCs in vivo, we used an oHSV bearing Fluc (oHSV-Fluc). MSCs freshly infected with oHSV-Fluc (MSC-oHSV-Fluc) were injected either via the ICA or i.v. into brain tumor-bearing mice and naive mice (non–tumor-bearing). An in vivo Fluc BLI signal indicating viral infection was detected as early as day 1 after MSC-oHSV-Fluc injection via the ICA, with a significant increase at day 5 in the brain tumor-bearing mice compared with the naive mice (Fig. 3*C*). The Fluc signals were detected exclusively in the brains of tumor-bearing mice, indicating that the majority of MSC-oHSV-Fluc cells home to tumor lesions in the brain upon ICA administration (*SI Appendix*, Fig. S6*A*). However, no Fluc BLI signal intensity was seen in the brain when MSC-oHSV-Fluc cells were injected i.v. into mice bearing MeWo-Rluc tumors. Instead, significant Fluc BLI intensity was seen in the lung, indicating that the vast majority of i.v.-injected cells were trapped in the lung (*SI Appendix*, Fig. S6*B*).

To further confirm the presence of oHSV within brain tumor lesions at cellular resolution after ICA injection, mice bearing MeWo-GFP tumors were ICA-injected with MSC-oHSV-mCh. Multicolor fluorescence imaging of serial brain sections from mice killed at different time points showed a rapid spread of oHSV-mCh emanating from a small population of MSC-oHSV-mCh cells within tumor deposits in the brain, with concomitant shrinkage of MeWo-GFP tumor areas within 120 h (Fig. 3*D*). In contrast, ICA injection of purified oHSV-mCh did not result in detectable mCherry fluorescence in melanoma-bearing mice, with no effects on GFP^+ tumor areas (Fig. 3*D*). Quantification of the fluorescent imaging results revealed a continuous increase in the oHSV-mCh-infected cell population in the brains of tumor-bearing mice with ICA-injected MSC-oHSV-mCh (Fig. 3*E*) and a concurrent decrease in the GFP^+ tumor cell population (Fig. 3*F*), a stark contrast to the observations with purified oHSV-mCh administration via the ICA.

X-gal staining on brain sections from mice bearing tumors injected with MSC-oHSV-mCh via the ICA revealed a time-dependent increase specifically in the oHSV reporter lacZ-positive pigmented tumors cells (Fig. 3*G*). Similar homing of MSC-oHSV-mCh was observed in mice bearing M12-GFP-Fluc tumor deposits in the brain (*SI Appendix*, Fig. S7). These data further confirm the transfer of oHSV from MSCs to tumor cells and the subsequent

infection of tumor cells while leaving the normal brain cells behind. These results show that intra-arterially administrated MSC-oHSV, but not purified oHSV, track and eliminate melanoma tumor cells in the brain.

MSC-oHSV has Therapeutic Efficacy in Both BRAF WT and Mutant Mouse Models of Melanoma Brain Metastasis. We next sought to determine the therapeutic potential of MSC-oHSV in mouse models of melanoma brain metastasis (Fig. 4*A*). BLI imaging revealed a significant remission of metastatic tumor burden in the brains of MeWo-FmC-bearing mice treated with MSC-oHSV compared with continuous tumor growth by treatment with uninfected MSCs (Fig. 4 *B* and *C*). This was further confirmed by a significant decrease in the number of pigmented lesions in the brains of the MSC-oHSV–treated group compared with controls (Fig. 4*D*), resulting in a significant survival benefit in treated mice (Fig. 4*E*). Similar studies were performed in mice bearing M12-FmC tumors. Treatment with MSC-oHSV significantly inhibited metastatic tumor growth in the brains of M12-FmC–bearing mice compared with controls (Fig. 4 *F* and *G*). This was further confirmed by a significant decrease in the number of Ki67^{+} proliferative tumor cells in the brain lesions of the MSC-oHSV–treated group compared with controls (Fig. 4*H*), resulting in prolonged survival

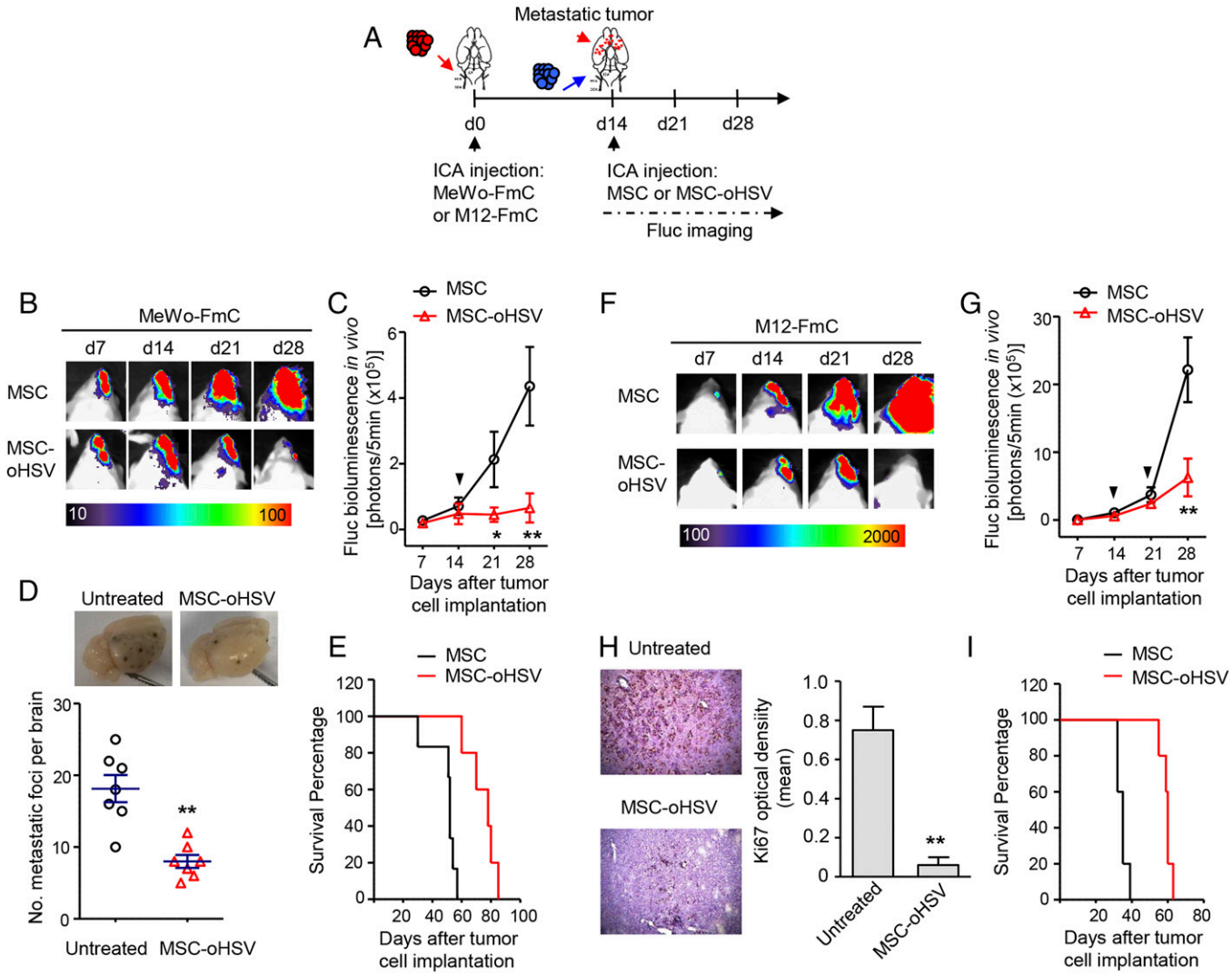

Fig. 4. ICA-delivered MSC-oHSV have therapeutic efficacy in melanoma brain metastasis derived from human BRAF WT and mutant melanoma lines. (*A*) Experimental outline. Red arrow indicates the route of tumor cell injection. Red arrowhead indicates the multiple tumor deposits in the brain. Blue arrow indicates the route for stem cell administration. (*B*) Representative bioluminescence images of MeWo-FmC–tumor bearing mice treated with MSC-oHSV or MSCs. (*C*) Plot of bioluminescence signal changes showing in vivo MeWo-FmC tumor growth after MSC-oHSV treatment. $*P < 0.05$, $**P < 0.01$ vs. the MSC-treated group ($n = 5$ mice per group). The black arrowhead indicates the time point of MSC or MSC-oHSV administration. (*D*) Representative images of pigmented metastatic foci in the brains of MSC-oHSV–treated and untreated mice at 4 wk after tumor cell implantation. $**P < 0.01$ vs. untreated control group ($n = 7$ mice per group). (*E*) Kaplan–Meier survival curves of MeWo-FmC tumor-bearing mice treated with MSC-oHSV or control MSCs. $P = 0.0014$ in the MSC-oHSV and control MSC comparison, log-rank test ($n = 6$ mice per group). (*F*) Representative bioluminescence images of M12-FmC tumor-bearing mice treated with MSC-oHSV or control MSCs. (*G*) Plot of bioluminescence signal changes showing in vivo M12-FmC tumor growth in MSC-oHSV– and control MSC-treated groups. $**P < 0.01$ vs. MSC-treated group ($n = 5$ mice per group). Black arrowheads indicate the two time points for MSC or MSC-oHSV administration. The second treatment was delivered via the contralateral ICA. (*H*) Immunohistochemistry-DAB images of Ki67 on brain sections and plot showing the optical density of Ki67 staining from MSC-oHSV–treated and untreated mice at 4 wk after tumor cell implantation. $**P < 0.01$ vs. untreated control group ($n = 3$ mice per group). (Magnification: 10×.) (*I*) Kaplan–Meier survival curves of M12-FmC tumor-bearing mice treated with MSC-oHSV or control MSCs. $P = 0.0019$ in the MSC-oHSV and control MSC comparison, log-rank test ($n = 5$ mice per group).

of MSC-oHSV–treated mice bearing M12-FmC brain tumors (Fig. 4*I*). These results demonstrate that intra-arterially administrated MSCs serve as robust cellular vehicles for delivering therapeutic oHSV to target and eliminate multiple metastatic deposits in the brain.

Characterization of the Syngeneic Melanoma Brain Metastasis Mouse Model. Although direct antitumor properties were originally considered the main mechanism of OVs, an increasing body of evidence suggests that the host immune response may be critical to the efficacy of oncolytic virotherapy (24). This may be mediated via innate immune effectors or via antiviral or antitumor adaptive cellular immune responses. Therefore, the use of an immunocompetent melanoma model to study the efficacy of MSC-oHSV is critical. We hypothesized that MSC-oHSV will synergize with immune checkpoint blockers, such as those that target the PD-1/PD-L1 pathway. To investigate the therapeutic efficacy of MSC-oHSV in combination with anti–PD-L1 immunotherapy, we successfully developed a syngeneic mouse model of melanoma brain metastasis by ICA injection of YUMM1.1 cells derived from an induced tumor in congenic C57BL/6 Tyr::CreER/Braf^{V600E}/^{wt}Cdkn2A$^{-/-}$Pten$^{-/-}$ mice. The YUMM1.1 cells were engineered to express GFP-Fluc (Y1.1-GFl; *SI Appendix*, Fig. S8*A*) and were ICA-injected in immunocompetent C57BL/6 mice. BLI on tumor-bearing mice revealed exclusive tumor growth in the brain (*SI Appendix*, Fig. S8 *B* and *C*) and the exponential growth of metastatic tumor in the brain at 3 wk after Y1.1-GFl implantation (Fig. 5 *A* and *B*), eventually resulting in mouse mortality. In vitro immunocytochemistry analysis showed that YUMM1.1 cells express both S100β, the melanoma biomarker protein, and PD-L1 (*SI Appendix*, Fig. S9*A*). In vivo, H&E staining showed the presence of multiple metastatic foci in mice brains (Fig. 5 *C*–*E*). Immunohistochemical analysis of brain sections from melanoma brain metastasis revealed an association of reactive astrocytes (GFAP$^+$) with metastatic tumor cells, suggesting an inflammatory response. Furthermore, S100β staining marked melanoma tumor cells, and diffuse PD-L1 and frequent Ki67-positive staining specifically seen in tumor lesions indicated that the metastatic melanoma cells are immunosuppressive and actively proliferative within the brain (Fig. 5 *F*–*K*). These data suggest that the syngeneic mouse model of melanoma brain metastasis is an ideal platform for studying the interaction between tumor cells and the tumor microenvironment, especially the immune system.

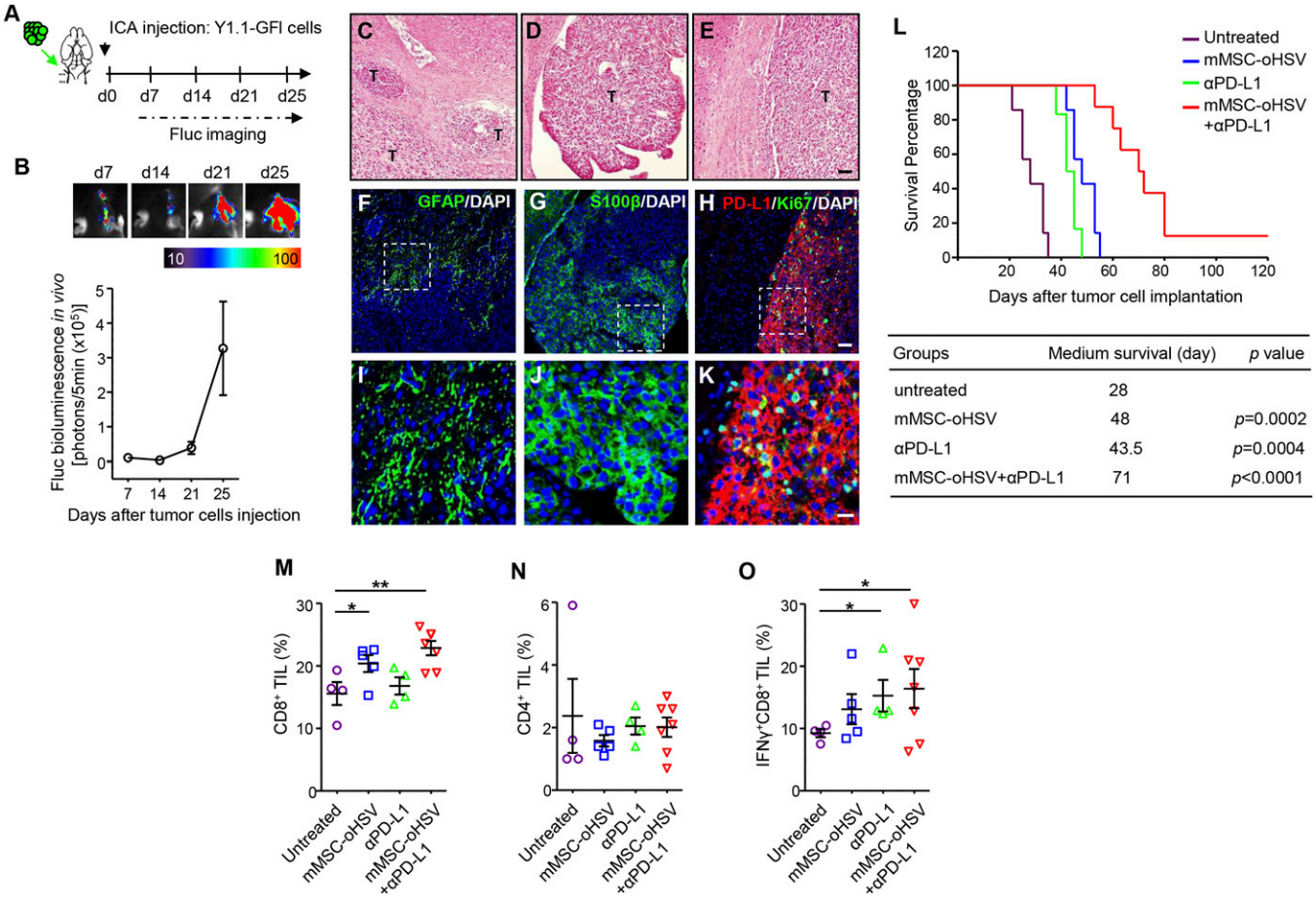

Groups	Medium survival (day)	*p* value
untreated	28	
mMSC-oHSV	48	*p*=0.0002
αPD-L1	43.5	*p*=0.0004
mMSC-oHSV+αPD-L1	71	*p*<0.0001

Fig. 5. Combined therapeutic efficacy of mouse MSC-oHSV and αPD-L1 in a syngeneic mouse model of melanoma brain metastasis. (*A*) Experimental outline. Green arrow indicates the route of tumor cell injection. Black arrow indicates the time point for tumor implantation. (*B*, *Top*) Representative bioluminescent images showing mice ICA-injected with Y1.1-GFl cells. (*B*, *Bottom*) Plot showing the in vivo bioluminescence intensity of metastatic tumor growth in the syngeneic mouse model (n = 5 mice). (*C*–*E*) H&E histology images showing multiple metastatic foci present in the brains of mice bearing melanoma brain metastases. T, tumor area. (Scale bar: 50 μm.) (*F*–*K*) Immunofluorescence analysis of mouse GFAP, S100β, PD-L1, and Ki67 in adjacent brain sections of mice bearing melanoma brain metastases (Scale bars: 50 μm in *F*–*H*, 20 μm in *I*–*K*). Nuclei were stained with DAPI. (*L*) Kaplan–Meier survival curves of melanoma brain metastasis-bearing mice treated with mMSC-oHSV (n = 7 mice), αPD-L1 (n = 6 mice), mMSC-oHSV + αPD-L1 (n = 8 mice), or untreated (n = 7 mice). The table presents the medium survival for each group and a comparison of the treated and untreated control groups (log-rank test). (*M*–*O*) Proportion of indicated cell populations determined by flow cytometry. Bars indicate mean values and SE. *P < 0.05, **P < 0.01 vs. untreated controls.

MSC-oHSV and Anti–PD-L1 Have Combined Therapeutic Efficacy in a Syngeneic Melanoma Brain Metastasis Mouse Model. We next examined the sensitivity of YUMM1.1 cells to oHSV infection in vitro. oHSV infection greatly decreased YUMM1.1 cell viability, which was associated with the production of oHSV over time (*SI Appendix*, Fig. S9 *B* and *C*). Coculture of YUMM1.1 and mouse MSCs freshly loaded with oHSV (mMSC-oHSV) resulted in a significant decrease in YUMM1.1 cell viability (*SI Appendix*, Fig. S9*D*). To test the therapeutic efficacy of mMSC-oHSV in combination with anti–PD-L1 antibody (αPD-L1) administration, mice bearing melanoma brain metastases were divided into four groups: control (untreated), treated with αPD-L1 (i.p. injection), mMSC-oHSV (ICA injection), and mMSC-oHSV + αPD-L1. A significant survival benefit was achieved by both αPD-L1 and mMSC-oHSV monotherapy; however, the combined therapy of mMSC-oHSV + αPD-L1 provided much greater survival extension than either monotherapy (Fig. 5*L*). In parallel, we also tested the efficacy of BRAF inhibitor PLX4720 on the survival of tumor-bearing mice. The results revealed that PLX4720 slightly prolonged mice survival; however, the tumor growth eventually led to mortality (*SI Appendix*, Fig. S10). Flow cytometry analysis of tumor-infiltrating T lymphocytes demonstrated a greatly increased $CD8^+$ fraction in the group of mice treated with mMSC-oHSV + αPD-L1 compared with the untreated control group (Fig. 5*M* and *SI Appendix*, Fig. S11), whereas no significant changes in the $CD4^+$ TIL subset were seen among the four groups (Fig. 5*N*). Within the $CD8^+$ cell population, more IFNγ-producing $CD8^+$ cells were found within the brain of mice treated with mMSC-oHSV + αPD-L1 compared with those of the untreated control group (Fig. 5*O*), suggesting that infiltrating cytotoxic $CD8^+$ TIL may play a role in eradicating metastatic tumor cells in the brain. These results strongly suggest that PD-L1 immune checkpoint blockade significantly improves the therapeutic efficacy of MSC-based oncolytic virotherapy in melanoma brain metastasis.

Discussion

In this study, we show that oHSV has a potent cell-killing effect in a broad spectrum of malignant melanoma lines. To explore the therapeutic efficacy of oHSV in melanoma brain metastasis, we created in vivo imageable mouse models of melanoma brain metastasis in both immunocompromised and immunocompetent mice. We demonstrate that ICA-delivered MSC-oHSV, but not purified oHSV, efficiently track metastatic tumor deposits in the brain, suppress brain tumor growth, and prolong survival in mouse models of melanoma brain metastasis. Furthermore, our studies demonstrate that the combination therapy of MSC-oHSV and anti–PD-L1 has improved therapeutic efficacy in syngeneic mouse model of melanoma brain metastasis, which is associated with an increased $CD8^+IFN\gamma^+$ TIL population.

Melanomas are molecularly heterogeneous tumors bearing different mutations and are resistant to a number of currently used chemotherapies (25, 26). In this study, we screened a panel of seven melanoma cell lines consisting of both established and patient-derived brain metastatic melanoma lines for their responses to oHSV infection and oncolysis. Our results reveal that oHSV infection has a consistent cell-killing effect on melanoma lines regardless of their BRAF mutational status, thus strongly supporting the use of oHSV for treating melanoma brain metastasis. Our screening results also demonstrated that the yields of oHSV in melanoma lines correlate with the efficiency of oHSV-mediated cell killing, suggesting that virus replication underlies the direct oncolytic effects. We also found that the oHSV yield in the patient-derived brain metastatic melanoma cell line M15 was relatively lower than that in the other melanoma lines, which correlated with less cell death in M15 cells treated with oHSV. Compared with MeWo, M12, and MSCs, M15 melanoma cells have decreased expression of Nectin-1 receptor, a major cell surface receptor for HSV entry (*SI Appendix*, Fig. S12), which may contribute to less permissive entry of oHSV into M15 cells. However, our data show that oHSV achieves better infection and spread in M15 cells at higher MOI (*SI Appendix*, Fig. S13 *A* and *B*). Based on our previous findings that the efficacy of oHSV-mediated cell killing can be significantly increased using a proapoptotic variant of oHSV, oHSV-TRAIL, in tumor lines that are less permissive to oHSV-mediated oncolysis (27), our future studies will focus on testing the efficacy of oHSV-TRAIL in such melanoma lines.

To test the therapeutic effects of oHSV in melanoma brain metastasis, we developed and extensively characterized in vivo imageable mouse models of melanoma brain metastasis that display the various features of brain metastasis observed in patients with advanced melanoma. Melanoma brain metastasis originates either directly from primary melanoma lesions or from metastatic lymph nodes and visceral lesions (13); therefore, we chose MeWo (derived from the metastatic lymph nodes in advanced melanoma) and M12 (derived from melanoma brain metastases) to mimic these two types of metastasis. These two melanoma lines are either *BRAF* WT or mutant ($BRAF^{V600E}$), the most frequent BRAF mutation seen in melanoma patients (28). Our results indicate that ICA injection of such lines results in the formation of clinically relevant mouse models that resemble the diverse features of metastatic melanoma, including widely disseminated numerous foci in the brain, aggressive and fatal growth, different mutational status of *BRAF*, and pigmented and nonpigmented lesions. These mouse models provide a unique and valuable platform for testing existing and novel therapeutic approaches for melanoma brain metastasis and help us better understand the pathogenesis of melanoma brain metastasis.

Previous studies typically used either intratumoral injection of oHSV into solid tumor lesions or systemic injection of high-dose oHSV (19, 29, 30). Given the multiple metastatic melanoma lesions in the brain, intratumoral injection into each single lesion is not a feasible approach. Systemic delivery of high-dose viruses carries a risk of virus-related toxicity (31). ICA delivery of oHSV has been explored previously in multiple glioblastoma and breast cancer brain metastasis models (32, 33); however, its efficiency is largely impeded by either antiviral activity present in plasma or undamaged BBB. Moreover, our studies have shown that ICA injection of purified oHSV (2×10^6 pfu) is unable to access multiple metastatic lesions in the brain. To overcome this limitation, we developed a strategy that uses MSCs as cellular carriers to shield oHSV from neutralization and achieve onsite delivery of oHSV to multiple tumor deposits in the brain. Stem cells, such as MSCs, are promising cell carriers for various antitumor viruses mainly because they can home to tumor deposits in the brain (34–37), can be easily isolated from patients and grown in culture, and have high metabolic activity, which is important for virus production (20, 38). Furthermore, MSCs are less immunogenic (39) and have been used in various clinical trials for different indications (40). In addition, MSCs also have been used as virus carriers in a phase 1 clinical trial in ovarian cancer patients (41). Using oHSV mutants bearing diagnostic proteins combined with bioluminescence and fluorescence imaging, our experiments reveal that MSCs act as oHSV carriers and track metastatic tumor deposits in the brain, ultimately releasing the oHSV. Our in vivo imaging data suggest that after ICA injection of MSC-oHSV-Fluc, virus replication initially occurs within infected MSCs, which releases oHSV-Fluc upon cell lysis, transfers oHSV to adjacent tumor cells, and results in subsequent virus replication in tumor cells. Comparison of the accessibilities of MSC-oHSV and purified oHSV to metastatic tumor lesions in the brain reveals that MSC-oHSV has superior tumor-tracking capability and results in a significant reduction in tumor foci and a survival advantage in mice bearing melanoma brain metastases. Importantly, ICA injection of MSC-oHSV was safe, and we did not observe any acute systemic toxicities or local adverse events, such as brain infarction. Although the mechanism of oHSV-mediated killing of MSCs

remains unclear, our results indicate that it is not mediated via apoptosis due to the absence of cleaved PARP, a hallmark of cell apoptosis (*SI Appendix*, Fig. S14).

The CNS is protected by the BBB and the blood-cerebrospinal fluid barrier, which prevent most therapeutic agents from entering into the brain. Although studies have shown increases in BBB permeability in various brain tumor models, it remains the key mitigating factor for delivering therapeutics into the CNS. Given that delivery of therapeutic agents to the tumors in the brain is a major challenge, significant efforts have been made to develop efficient delivery routes to brain tumors, which include both invasive and noninvasive administration strategies (42). In a previous study, we showed that local implantation of encapsulated MSCs loaded with oHSV have therapeutic efficacy in mouse models of resected brain tumors (21). Recent studies have shown that i.v. injected MSC-oHSV have therapeutic efficacy in treating lung metastatic tumors (43). These studies imply that i.v.-injected MSC-oHSV would be more suitable for treating both primary and metastatic tumors in the lungs as opposed to the tumors in the brain. Therefore, exploring alternate routes of administration of MSC-oHSV to tumors in the brain was critical.

Immune checkpoint blockade is a major advance in recent cancer therapy, especially for the treatment of metastatic melanoma (44), which is typically immunogenic, likely due to the large numbers of UV-associated mutations (45). Two monoclonal antibodies that block PD-1/PD-L1 interactions (pembrlizumab and nivolumab) have shown objective responses in 30∼40% of patients with melanoma brain metastasis (46, 47). oHSV represents a novel approach to tumor immunotherapy and is an attractive option based on its ability to preferentially target, infect, and replicate in cancer cells. Furthermore, oHSV viral genomes can be easily attenuated to limit host pathogenicity or engineered to express immune-potentiating genes to enhance the host antitumor immune response (48). Because PD-1 is activated mostly at tumor sites or other areas of active immune response, the side effects of anti–PD-1/PD-L1 therapy tend to be less severe than those associated with anti–CTLA-4 antibodies, which potentially affect all circulating T cells in the body and thus can cause significant, albeit manageable, autoimmune side effects (49). Meanwhile, our results showed strong PD-L1 expression in melanoma brain metastasis in the syngeneic mouse model. We thus chose to use an anti–PD-L1 immune-checkpoint blocker to antagonize the immune suppression posed by metastatic melanoma cells.

Our study investigated the therapeutic efficacy of MSC-oHSV in combination with anti–PD-L1 for melanoma brain metastasis. We found that $CD8^+IFN\gamma^+$ TIL population was associated with the survival benefits achieved by the combination therapy of MSC-oHSV plus anti–PD-L1, suggesting that cytotoxic $CD8^+$ TIL may play a critical role in killing metastatic melanoma cells in the brain, likely via activation of IFNγ-related signaling pathways. Release of IFNγ at the tumor site could limit oHSV spread but trigger a variety of beneficial responses, such as activation of other immune cell subsets, up-regulation of MHC class I, and antiangiogenesis. The transient nature of IFNγ secretion likely would limit the detrimental impacts of IFNγ-induced inflammatory reactions in the brain. The overall cellular responses to the oHSV infection, coupled with the release of tumor antigens by virally infected dying tumor cells into the tumor microenvironment, attract innate and adaptive immune cells, including tumor-specific $CD4^+$ and $CD8^+$ T cells. This oHSV infection-mediated response makes virotherapy an ideal modality to combine with immune checkpoint blockers to achieve a more durable response and outcome. Our data suggest that the increased population of $CD8^+IFN\gamma^+$ TIL represents a beneficial antitumor immune response elicited by MSC-oHSV therapy for melanoma brain metastasis.

In conclusion, we have shown that intra-arterial delivery of MSC-loaded oHSV can effectively track and kill metastatic melanoma cells in the brain, and that combination therapy with an immune checkpoint blocker boosts the therapeutic efficacy of MSC-oHSV. Thus, our study warrants clinical testing of MSC-oHSV alone or in combination with immune checkpoint blockers for patients with melanoma brain metastases. Attributed to their innate tumor tropism, stem cells carrying oHSV have been shown to target tumor lesions in the lung and prevent metastases upon i.v. injection (43). Based on previous findings and our present findings, stem cell-based oncolytic virotherapies could have the potential to be broadly applicable in targeting metastatic lesions in organs such as the liver, colon, and lung.

Materials and Methods

Detailed information on the materials and methods used in this study is provided in *SI Appendix*. All of the animal studies were approved by Massachusetts General Hospital's institutional review board.

Cell Lines. MeWo, SK-Mel-2, SK-Mel-28, MALME-3M, and YUMM1.1 melanoma cells were cultured in DMEM (MeWo, MALME-3M, and YUMM1.1) or RPMI (SK-Mel-2 and SK-Mel-28) supplemented with 10% FBS and 1% penicillin-streptomycin. TXM-13 cells were kindly provided by I. J. Fidler and cultured in TXM medium (MEM supplemented with 10% FBS, 1% vitamin, 1% sodium pyruvate, 1% nonessential amino acid, and 1% penicillin-streptomycin). M12 and M15 patient-derived melanoma brain metastatic lines (kindly provided by J. Sarkaria, Mayo Clinic, Rochester) were cultured in DMEM supplemented with 10% FBS and 1% penicillin-streptomycin. Human and mouse MSCs were cultured in NutriStem XF Medium and MesenCult MSC Basal Medium, respectively. Normal human astrocytes were grown in DMEM supplemented with 10% FBS and 1% penicillin-streptomycin.

Engineered Viral Vectors, Viral Packaging, and Transduction of Tumor Cells. The following lentiviral constructs were used in this study: Pico2-Fluc-mCherry and Pico2-Fluc-GFP. Lentiviral packaging was performed by transfection of 293T cells as described previously (50). MeWo and M12 cells were transduced at an MOI of 5 in medium containing protamine sulfate (10 μg/mL). All cells were visualized by fluorescence microscopy for GFP or mCherry expression to confirm transduction. oHSV-mCherry and oHSV-Fluc were previously generated by cloning mCherry or Fluc cDNA under the HSV IE4/5 immediate early promoter or CMV promoter, respectively, using site-specific recombination between the G47delta BAC and the shuttle plasmid (27, 51). All of the recombinant oHSVs express *Escherichia coli* lacZ driven by endogenous ICP6 promoter.

Statistical Analysis. Data were analyzed using the Student *t* test when comparing two groups and ANOVA when comparing more than two groups. Data were plotted as mean ± SEM, and differences were considered significant at $P < 0.05$. Survival curves were compared using the log-rank test. Analyses were done using GraphPad Prism 5.01.

ACKNOWLEDGMENTS. We thank Mark Schroeder and Jan Sarkaria for providing patient-derived M12 and M15 tumor lines, Yohei Kitamura and Deepak Bhere for helping with the in vivo M12 tumor model, Jennifer Lo for assisting with the melanoma cell culture, and Ravi Mylvaganam for FACS analysis. This work was supported by Department of Defense Idea Award CA140744 (to K.S.) and National Institutes of Health Grants R01 CA204720 (to K.S.), P01 CA163222 (to D.F.).

1. Siegel RL, Miller KD, Jemal A (2016) Cancer statistics, 2016. *CA Cancer J Clin* 66:7–30.
2. Fidler IJ, Schackert G, Zhang RD, Radinsky R, Fujimaki T (1999) The biology of melanoma brain metastasis. *Cancer Metastasis Rev* 18:387–400.
3. Sampson JH, Carter JH, Jr, Friedman AH, Seigler HF (1998) Demographics, prognosis, and therapy in 702 patients with brain metastases from malignant melanoma. *J Neurosurg* 88:11–20.
4. Long GV, et al. (2012) Dabrafenib in patients with Val600Glu or Val600Lys BRAF-mutant melanoma metastatic to the brain (BREAK-MB): A multicentre, open-label, phase 2 trial. *Lancet Oncol* 13:1087–1095.
5. Ramanujam S, Schadendorf D, Long GV (2015) Systemic therapies for melanoma brain metastases: Which drug for whom and when? *Chin Clin Oncol* 4:25.
6. Tas F (2012) Metastatic behavior in melanoma: Timing, pattern, survival, and influencing factors. *J Oncol* 2012:647684.
7. Ramakrishna N, Margolin KA (2013) Multidisciplinary approach to brain metastasis from melanoma: Local therapies for central nervous system metastases. *Am Soc Clin Oncol Educ Book* 2013:399–403.
8. Brown P, et al. (2015) A phase III randomized trial of whole brain radiation therapy (WBRT) in addition to radiosurgery (SRS) in patients with 1 to 3 brain metastases. *J Clin Oncol* 33:15.

9. Bentolila LA, et al. (2016) Imaging of angiotropism/vascular co-option in a murine model of brain melanoma: Implications for melanoma progression along extravascular pathways. *Sci Rep* 6:23834.
10. Zou Z, et al. (2016) Convection-enhanced delivery of sorafenib and suppression of tumor progression in a murine model of brain melanoma through the inhibition of signal transducer and activator of transcription 3. *J Neurosurg* 124:1310–1318.
11. Bahrambeigi V, Ahmadi N, Salehi R, Javanmard SH (2015) Genetically modified murine adipose-derived mesenchymal stem cells producing interleukin-2 favor B16F10 melanoma cell proliferation. *Immunol Invest* 44:216–236.
12. Fonkem E, et al. (2012) Melanoma brain metastasis: Overview of current management and emerging targeted therapies. *Expert Rev Neurother* 12:1207–1215.
13. Fidler IJ (2015) The biology of brain metastasis: Challenges for therapy. *Cancer J* 21: 284–293.
14. Liu TC, Galanis E, Kirn D (2007) Clinical trial results with oncolytic virotherapy: A century of promise, a decade of progress. *Nat Clin Pract Oncol* 4:101–117.
15. Lawler SE, Chiocca EA (2015) Oncolytic virus-mediated immunotherapy: A combinatorial approach for cancer treatment. *J Clin Oncol* 33:2812–2814.
16. MacKie RM, Stewart B, Brown SM (2001) Intralesional injection of herpes simplex virus 1716 in metastatic melanoma. *Lancet* 357:525–526.
17. Andtbacka RH, et al. (2015) Talimogene laherparepvec improves durable response rate in patients with advanced melanoma. *J Clin Oncol* 33:2780–2788.
18. Harrington KJ, et al. (2015) Clinical development of talimogene laherparepvec (T-VEC): A modified herpes simplex virus type-1-derived oncolytic immunotherapy. *Expert Rev Anticancer Ther* 15:1389–1403.
19. Russell SJ, Peng KW, Bell JC (2012) Oncolytic virotherapy. *Nat Biotechnol* 30:658–670.
20. Shah K (2012) Mesenchymal stem cells engineered for cancer therapy. *Adv Drug Deliv Rev* 64:739–748.
21. Duebgen M, et al. (2014) Stem cells loaded with multimechanistic oncolytic herpes simplex virus variants for brain tumor therapy. *J Natl Cancer Inst* 106:dju090.
22. Stuckey DW, Shah K (2014) Stem cell-based therapies for cancer treatment: Separating hope from hype. *Nat Rev Cancer* 14:683–691.
23. Tsao H, Goel V, Wu H, Yang G, Haluska FG (2004) Genetic interaction between NRAS and BRAF mutations and PTEN/MMAC1 inactivation in melanoma. *J Invest Dermatol* 122:337–341.
24. Kaufman HL, Kohlhapp FJ, Zloza A (2015) Oncolytic viruses: A new class of immunotherapy drugs. *Nat Rev Drug Discov* 14:642–662.
25. Tsao H, Chin L, Garraway LA, Fisher DE (2012) Melanoma: From mutations to medicine. *Genes Dev* 26:1131–1155.
26. Lo JA, Fisher DE (2014) The melanoma revolution: From UV carcinogenesis to a new era in therapeutics. *Science* 346:945–949.
27. Tamura K, et al. (2013) Multimechanistic tumor targeted oncolytic virus overcomes resistance in brain tumors. *Mol Ther* 21:68–77.
28. Davies H, et al. (2002) Mutations of the BRAF gene in human cancer. *Nature* 417: 949–954.
29. Varghese S, et al. (2007) Systemic therapy of spontaneous prostate cancer in transgenic mice with oncolytic herpes simplex viruses. *Cancer Res* 67:9371–9379.
30. Kulu Y, et al. (2009) Comparison of intravenous versus intraperitoneal administration of oncolytic herpes simplex virus 1 for peritoneal carcinomatosis in mice. *Cancer Gene Ther* 16:291–297.
31. Ferguson MS, Lemoine NR, Wang Y (2012) Systemic delivery of oncolytic viruses: Hopes and hurdles. *Adv Virol* 2012:805629.
32. Ikeda K, et al. (1999) Oncolytic virus therapy of multiple tumors in the brain requires suppression of innate and elicited antiviral responses. *Nat Med* 5:881–887.
33. Liu R, Martuza RL, Rabkin SD (2005) Intracarotid delivery of oncolytic HSV vector G47Delta to metastatic breast cancer in the brain. *Gene Ther* 12:647–654.
34. Tang Y, et al. (2003) In vivo tracking of neural progenitor cell migration to glioblastomas. *Hum Gene Ther* 14:1247–1254.
35. Aboody KS, et al. (2000) Neural stem cells display extensive tropism for pathology in adult brain: Evidence from intracranial gliomas. *Proc Natl Acad Sci USA* 97: 12846–12851.
36. Shah K, et al. (2005) Glioma therapy and real-time imaging of neural precursor cell migration and tumor regression. *Ann Neurol* 57:34–41.
37. Sasportas LS, et al. (2009) Assessment of therapeutic efficacy and fate of engineered human mesenchymal stem cells for cancer therapy. *Proc Natl Acad Sci USA* 106: 4822–4827.
38. Willmon C, et al. (2009) Cell carriers for oncolytic viruses: Fed Ex for cancer therapy. *Mol Ther* 17:1667–1676.
39. Jacobs SA, Roobrouck VD, Verfaillie CM, Van Gool SW (2013) Immunological characteristics of human mesenchymal stem cells and multipotent adult progenitor cells. *Immunol Cell Biol* 91:32–39.
40. Kim N, Cho SG (2013) Clinical applications of mesenchymal stem cells. *Korean J Intern Med* 28:387–402.
41. Mader EK, et al. (2013) Optimizing patient-derived mesenchymal stem cells as virus carriers for a phase I clinical trial in ovarian cancer. *J Transl Med* 11:20.
42. Laquintana V, et al. (2009) New strategies to deliver anticancer drugs to brain tumors. *Expert Opin Drug Deliv* 6:1017–1032.
43. Leoni V, et al. (2015) Systemic delivery of HER2-retargeted oncolytic-HSV by mesenchymal stromal cells protects from lung and brain metastases. *Oncotarget* 6: 34774–34787.
44. Brahmer JR, et al. (2012) Safety and activity of anti–PD-L1 antibody in patients with advanced cancer. *N Engl J Med* 366:2455–2465.
45. Cancer Genome Atlas Network (2015) Genomic classification of cutaneous melanoma. *Cell* 161:1681–1696.
46. Robert C, et al.; KEYNOTE-006 Investigators (2015) Pembrolizumab versus ipilimumab in advanced melanoma. *N Engl J Med* 372:2521–2532.
47. Wolchok JD, et al. (2013) Nivolumab plus ipilimumab in advanced melanoma. *N Engl J Med* 369:122–133.
48. Cattaneo R, Miest T, Shashkova EV, Barry MA (2008) Reprogrammed viruses as cancer therapeutics: Targeted, armed and shielded. *Nat Rev Microbiol* 6:529–540.
49. Topalian SL, Drake CG, Pardoll DM (2015) Immune checkpoint blockade: A common denominator approach to cancer therapy. *Cancer Cell* 27:450–461.
50. Shah K, et al. (2008) Bimodal viral vectors and in vivo imaging reveal the fate of human neural stem cells in experimental glioma model. *J Neurosci* 28:4406–4413.
51. Cheema TA, et al. (2013) Multifaceted oncolytic virus therapy for glioblastoma in an immunocompetent cancer stem cell model. *Proc Natl Acad Sci USA* 110:12006–12011.

Fig. S1

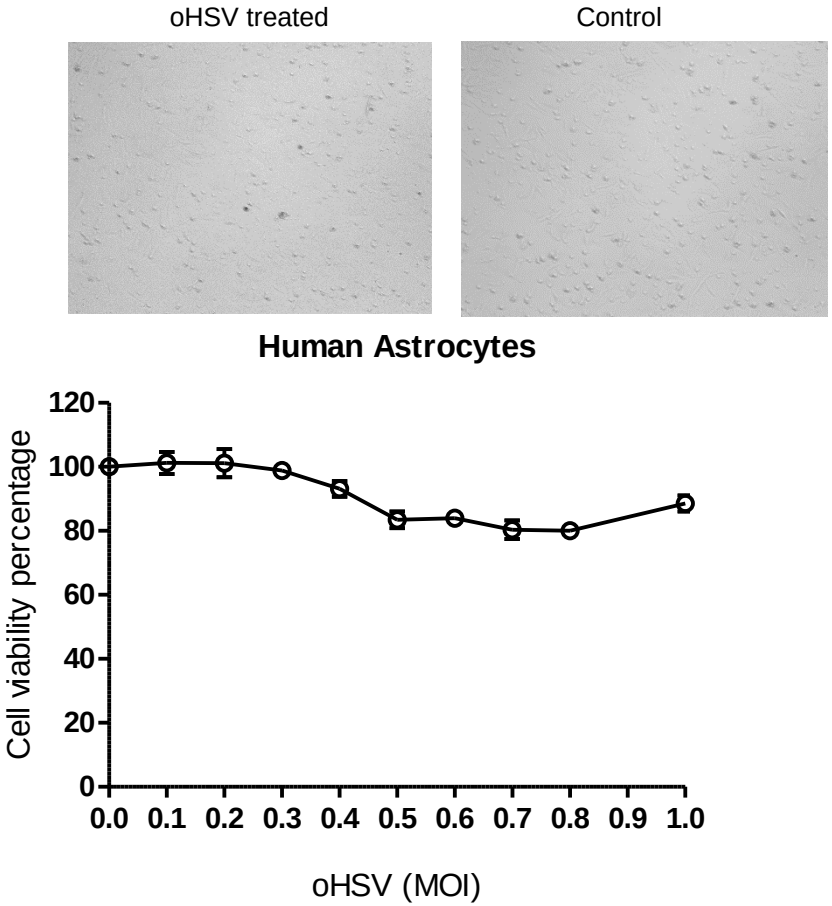
oHSV treated
Control
Human Astrocytes
Cell viability percentage
120
100
80
60
40
20
0
0.0 0.1 0.2 0.3 0.4 0.5 0.6 0.7 0.8 0.9 1.0
oHSV (MOI)

Fig. S2

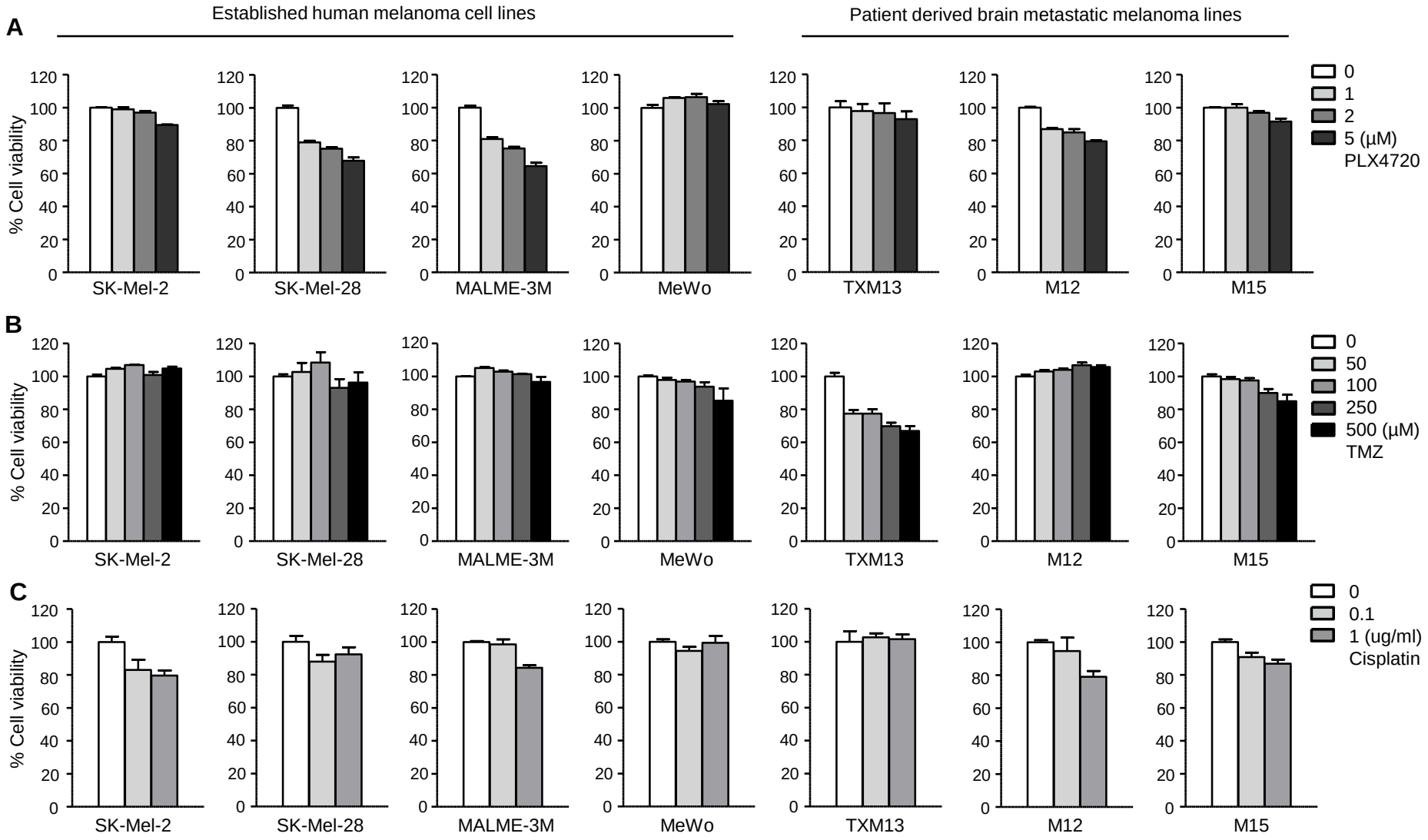
A
Established human melanoma cell lines
Patient derived brain metastatic melanoma lines
% Cell viability
SK-Mel-2
SK-Mel-28
MALME-3M
MeWo
TXM13
M12
M15
0
1
2
5 (µM)
PLX4720
B
0
50
100
250
500 (µM)
TMZ
C
0
0.1
1 (ug/ml)
Cisplatin

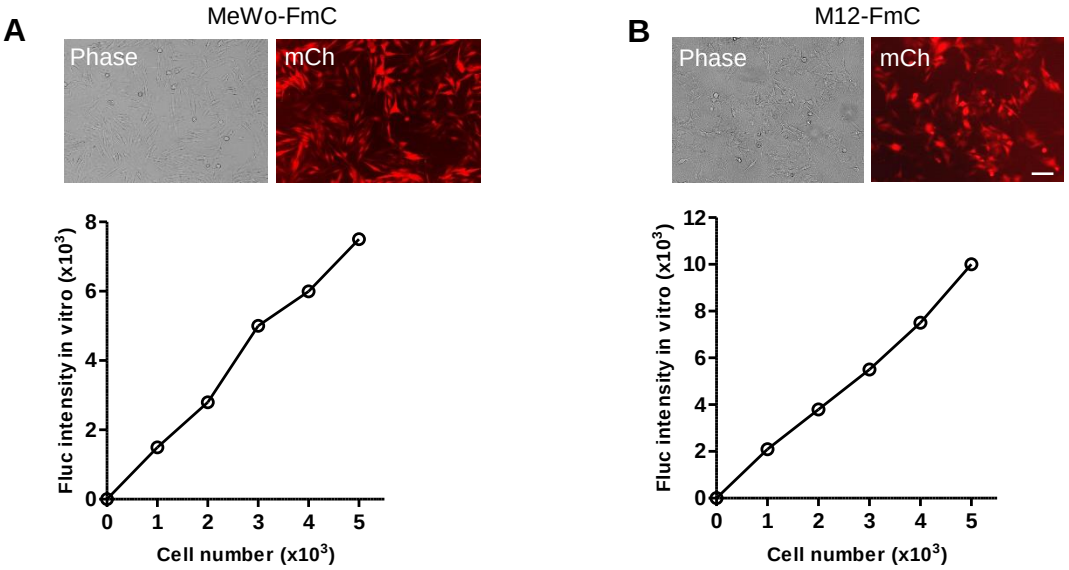
A
MeWo-FmC
Phase
mCh
Fluc intensity in vitro (x10^3)
Cell number (x10^3)
B
M12-FmC
Phase
mCh
Fluc intensity in vitro (x10^3)
Cell number (x10^3)

Fig. S4

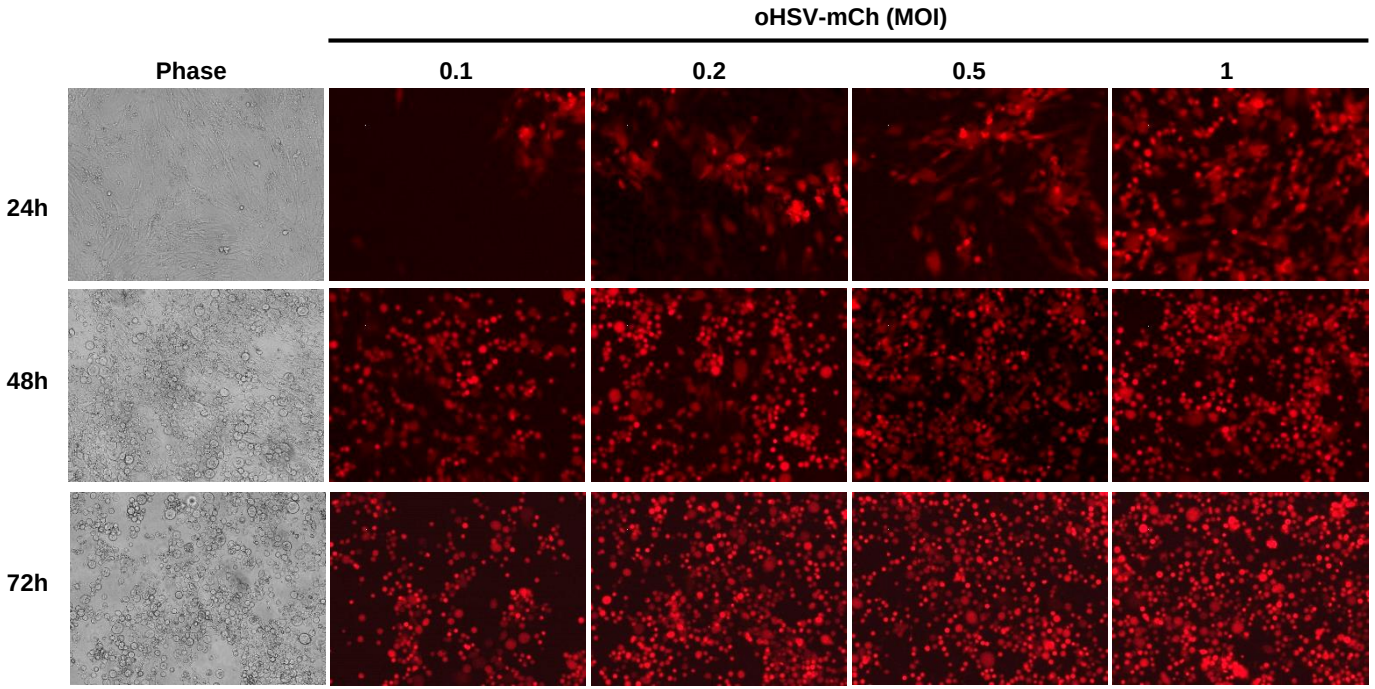

Fig. S5

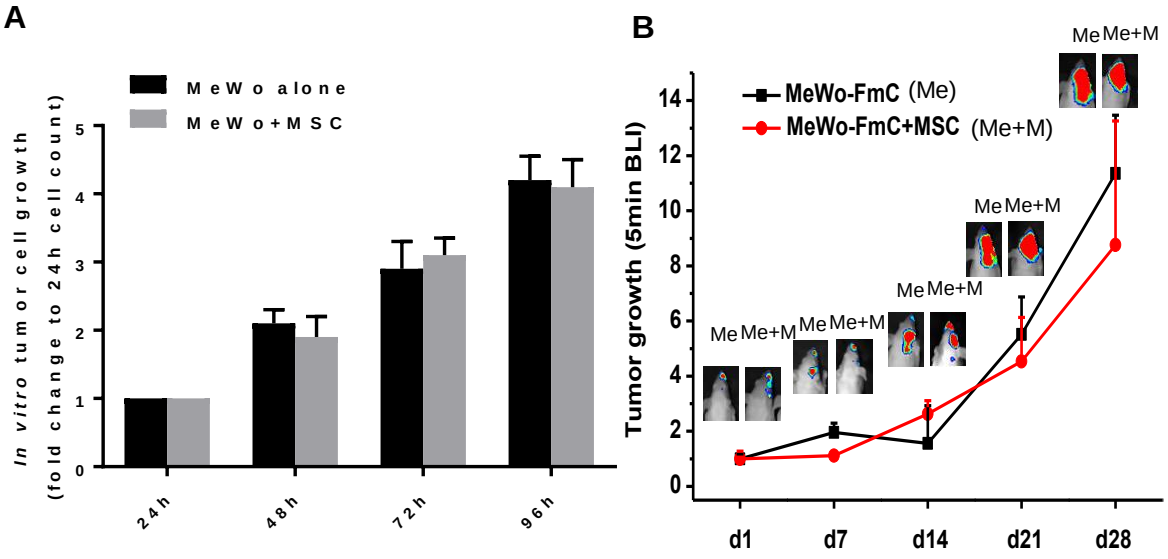
A
MeWo alone
MeWo+MSC
In vitro tumor cell growth
(fold change to 24h cell count)
0
1
2
3
4
5
24h
48h
72h
96h
B
MeWo-FmC (Me)
MeWo-FmC+MSC (Me+M)
Tumor growth (5min BLI)
0
2
4
6
8
10
12
14
d1
d7
d14
d21
d28
Me
Me+M

Fig. S6

A

Day 5, ICA injected MSC-oHSV-Fluc in brain tumor bearing mice

Fluc Imaging

B

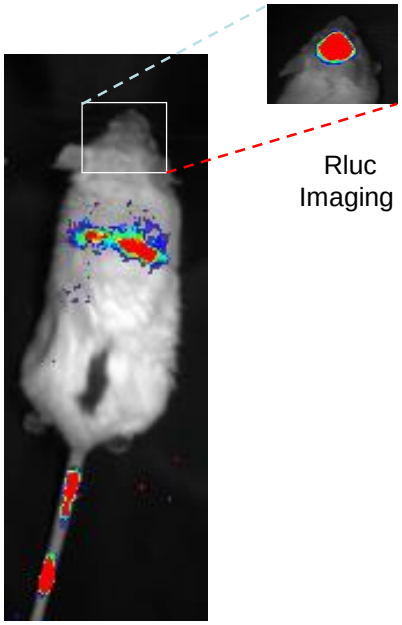

Rluc Imaging

Fluc Imaging

Fig. S7

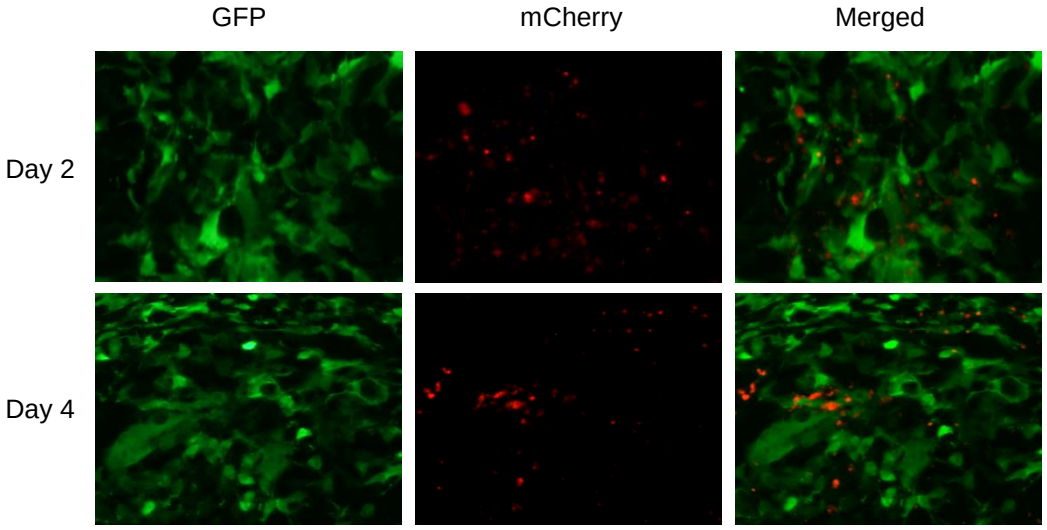

Fig. S8

A

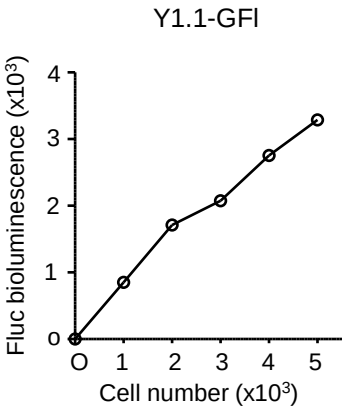

B

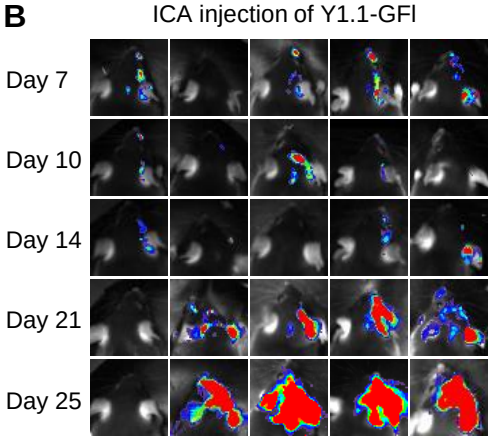

C

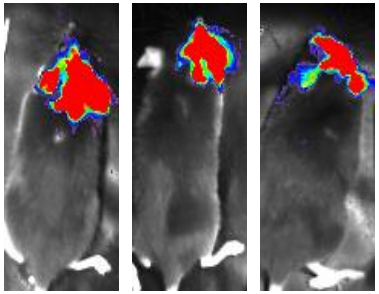

Day 25 after ICA injection of Y1.1-GFl
Whole BLI images

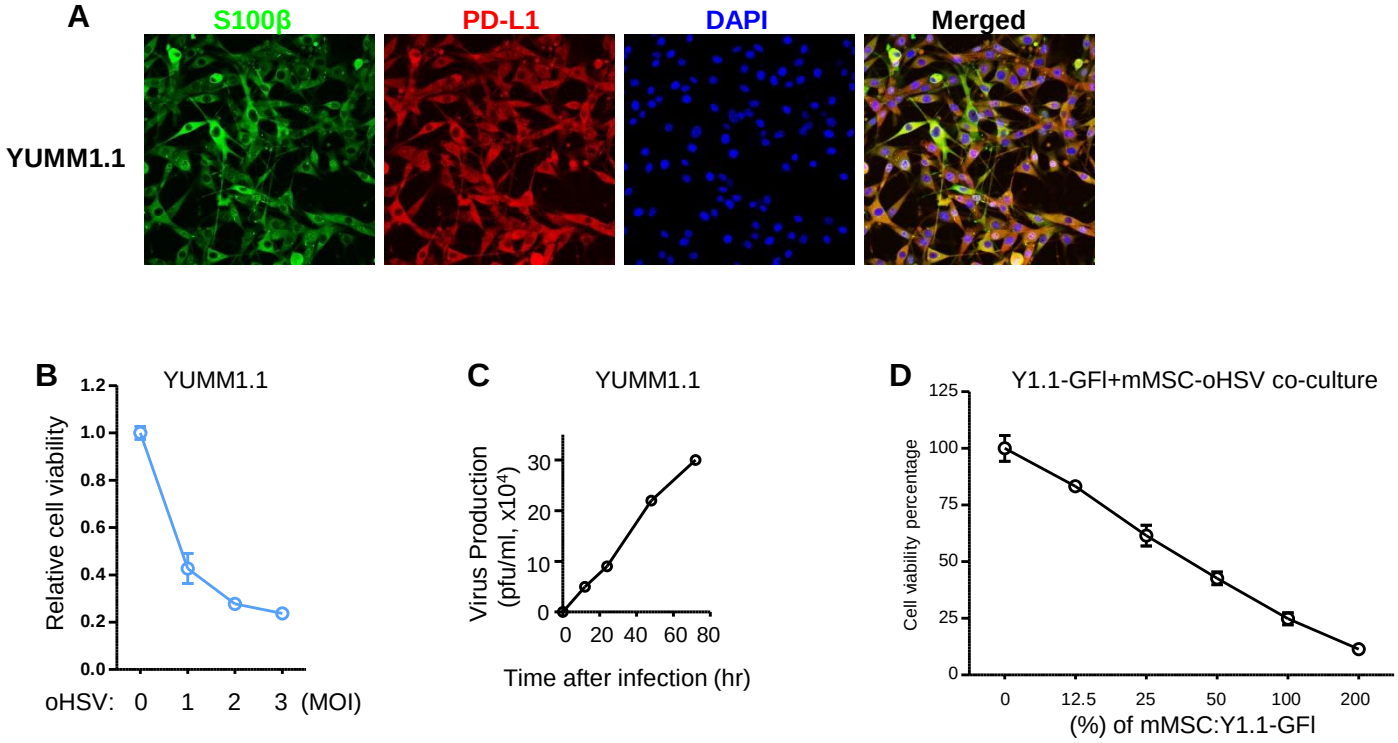
A
S100β
PD-L1
DAPI
Merged
YUMM1.1
B
YUMM1.1
Relative cell viability
1.2
1.0
0.8
0.6
0.4
0.2
0.0
oHSV: 0 1 2 3 (MOI)
C
YUMM1.1
Virus Production (pfu/ml, x10⁴)
30
20
10
0
0 20 40 60 80
Time after infection (hr)
D
Y1.1-GFl+mMSC-oHSV co-culture
Cell viability percentage
125
100
75
50
25
0
0 12.5 25 50 100 200
(%) of mMSC:Y1.1-GFl

Fig. S10

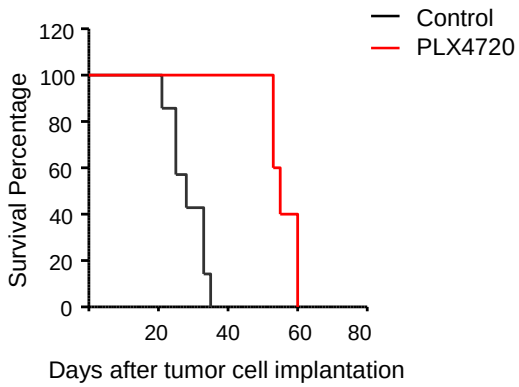
Control
PLX4720
120
100
80
60
40
20
0
Survival Percentage
20
40
60
80
Days after tumor cell implantation

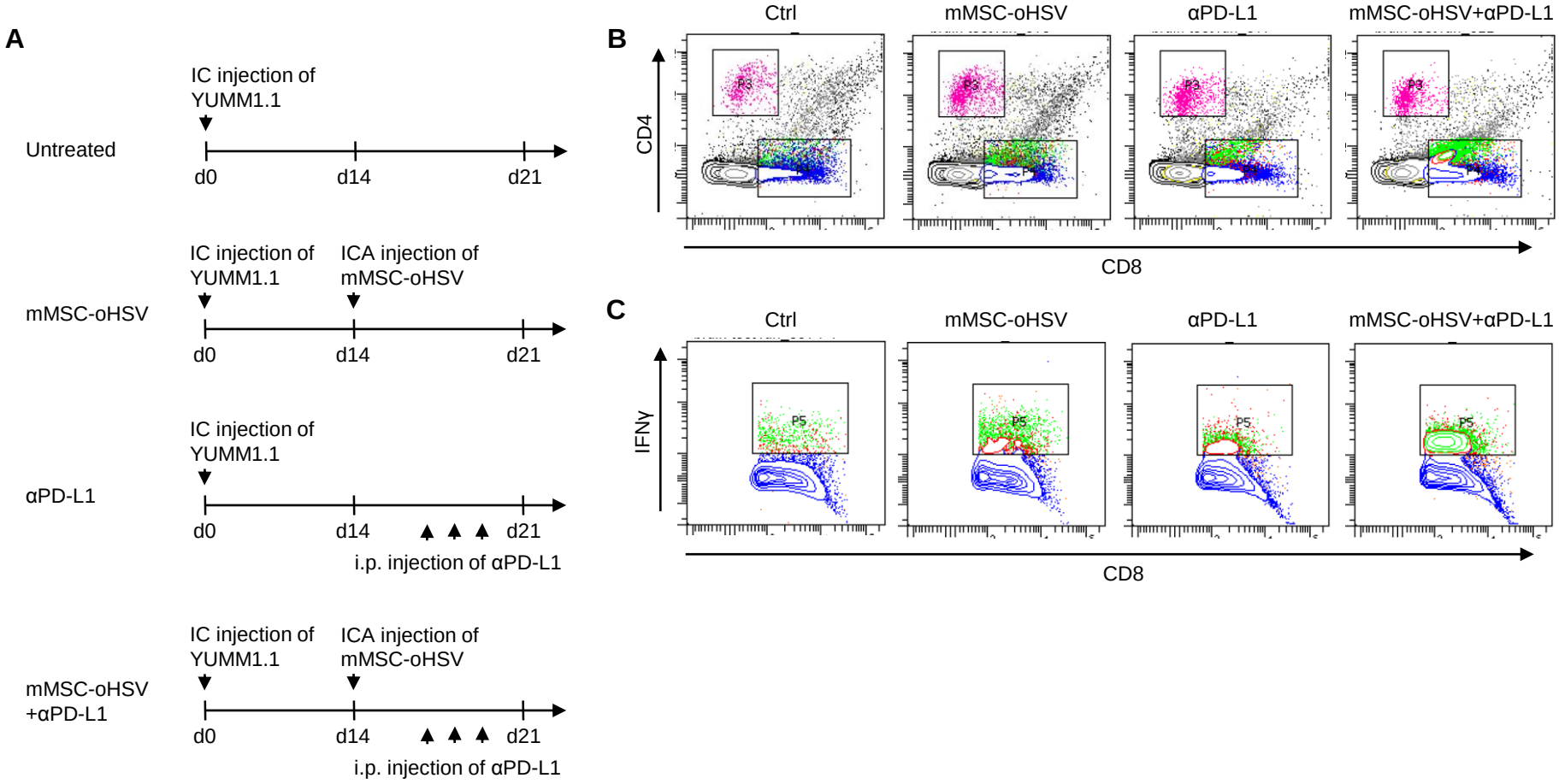
A
IC injection of YUMM1.1
Untreated
d0
d14
d21
IC injection of YUMM1.1
ICA injection of mMSC-oHSV
mMSC-oHSV
d0
d14
d21
IC injection of YUMM1.1
αPD-L1
d0
d14
d21
i.p. injection of αPD-L1
IC injection of YUMM1.1
ICA injection of mMSC-oHSV
mMSC-oHSV +αPD-L1
d0
d14
d21
i.p. injection of αPD-L1
B
Ctrl
mMSC-oHSV
αPD-L1
mMSC-oHSV+αPD-L1
CD4
CD8
C
Ctrl
mMSC-oHSV
αPD-L1
mMSC-oHSV+αPD-L1
IFNγ
CD8

Fig. S12

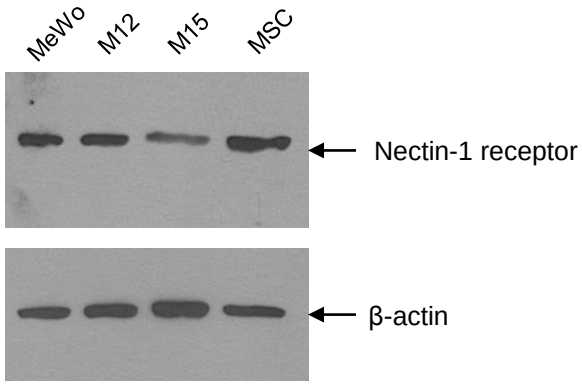

Fig. S13

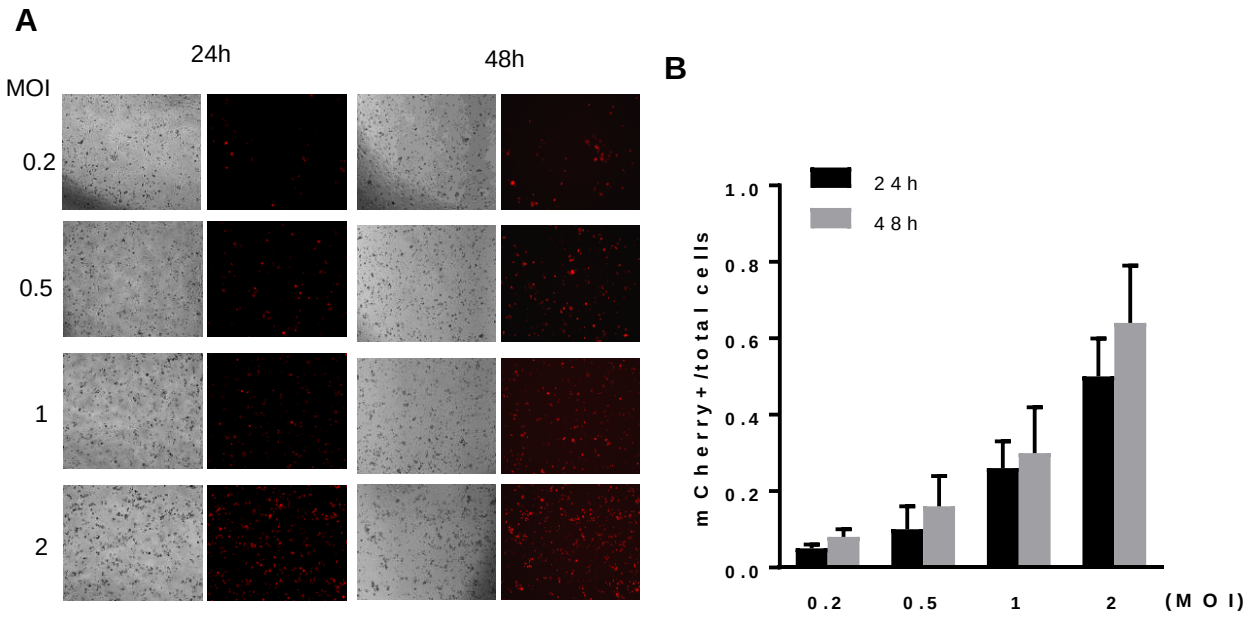
A
24h
48h
MOI
0.2
0.5
1
2
B
24h
48h
mCherry+/total cells
1.0
0.8
0.6
0.4
0.2
0.0
0.2
0.5
1
2
(MOI)

Fig. S14

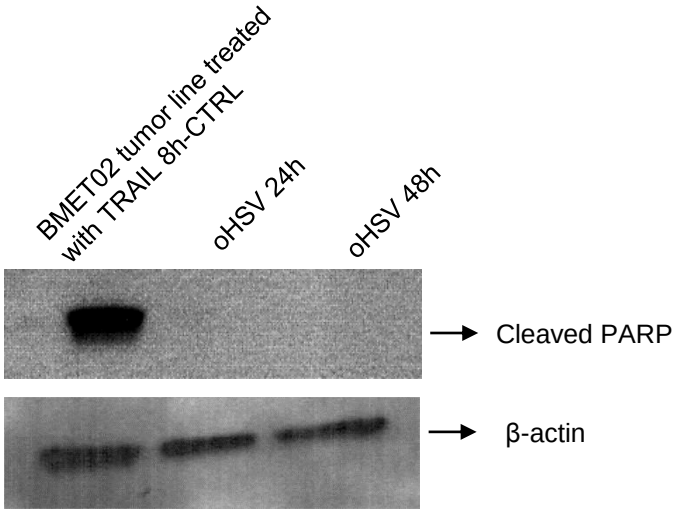
BMET02 tumor line treated with TRAIL 8h-CTRL
oHSV 24h
oHSV 48h
Cleaved PARP
β-actin

Supplementary Figure legends

Supplementary Figure 1. Plot and representative images showing the cell viability of human astrocytes infected with oHSV at different MOI 4 days post infection.

Supplementary Figure 2. Responses of multiple human melanoma lines to PLX4720, TMZ and Cisplatin. Plots showing cell viabilities of melanoma lines treated with PLX4720 (A), TMZ (B) and low dose Cisplatin (C) at indicated concentrations.

Supplementary Figure 3. Characterization of engineered MeWo-FmC and M12-FmC. (A, B) Upper, representative phase and fluorescent images of engineered MeWo-FmC and M12-FmC lines. Lower, correlation between cell number and *in vitro* Fluc bioluminescence signal was analyzed.

Supplementary Figure 4. Representative phase and fluorescent images of human MSC transduced with oHSV-mCh at different MOI over time.

Supplementary Figure 5. (A) Plot showing MeWo-GFP tumor cell growth over time in the presence and absence of MSC in co-culture settings. (B) *In vivo* bioluminescence imaging of MeWo-FmC tumor growth over time in mice brains with or without ICA injection of MSC.

Supplementary Figure 6: (A) Fluc bioluminescent images of brain tumor bearing mice treated with ICA injection of MSC-oHSV-Fluc. (B) Human MSC expressing firefly luciferase (Fluc) were incubated with oHSV for 6 hours and injected via tail vein in mice bearing MeWo-Rluc tumors. Fluc bioluminescent image showing the fate of MSC 24 hrs post-injection. (Inset) Rluc bioluminescent image showing MeWo-Rluc tumor in the brain.

Supplementary Figure 7. Fluorescent images from brain sections of mice showing the population of M12-GFP-Fluc tumor cells (GFP^+) and MSC-oHSV-mCh cells (mCh^+) at indicated time points post-ICA injection of MSC-oHSV-mCh in M12-GFP-Fluc tumor bearing mice.

Supplementary Figure 8. Characterization of engineered Y1.1-GFl. (A) Linear correlation between Y1.1 engineered to express GFP-firefly luciferase (Y1.1-GFl) cell number and *in vitro* Fluc bioluminescence

signal. (B) Representative bioluminescent images of mice ICA injected with Y1.1-GFl at various time points post tumor cells implantation. (C) Whole body BLI images of mice with ICA injected Y1.1-GFl.

Supplementary Figure 9. Characterization of YUMM1.1 *in vitro*. (A) Immunocytochemistry analysis of S100β and PD-L1 staining in YUMM1.1 cells. (B) Cell viability of YUMM1.1 cells infected with oHSV at indicated MOI. (C) Plots showing oHSV virus production within YUMM1.1 cells infected with oHSV at MOI=0.5 over time. (D) Plot showing cell viability of Y1.1-GFl cells in co-cultures of Y1.1-GFl and mMSC-oHSV at indicated portions.

Supplementary Figure 10. Kaplan-Meier survival curves of melanoma brain metastasis bearing mice treated with PLX4720 (low dose chow food, n=5 mice) or untreated (n=7 mice). p=0.0011 in PLX4720 and control comparison, log-rank test.

Supplementary Figure 11. Flow cytometry analysis of tumor infiltrating lymphocytes in syngeneic mouse model. (A) Experiment outline. (B, C) Representative density plots for CD4, CD8 and IFNγ staining from the four groups of mice, tumor only (untreated control group), tumor+mMSC-oHSV, tumor+αPD-L1 and tumor+mMSC-oHSV+αPD-L1 treated groups.

Supplementary Figure 12. Western blot analysis showing nectin-1 receptor expression levels in MeWo, M12, M15 melanoma lines and human MSC.

Supplementary Figure 13. (A) Representative images of M15 infected with oHSV at indicated MOIs over time. (B) Plot showing the percentage of oHSV infected M15 cell populations at indicated time points.

Supplementary Figure 14. Western blot analysis showing cleaved PARP levels in both MeWo cells treated with oHSV after 24 and 48 hrs and in breast cancer cell line, BMET02 tumor line treated with TRAIL for 8 hrs as a positive control for cleaved PARP.

Supplementary Methods

Cell viability assays and oHSV production assay: The effect of oHSV on tumor cell viability and astrocytes was measured using CellTiterGlo (Promega, Madison, WI, USA) 4 days post virus infection with different MOI. All experiments were performed in triplicates. For the viral production assay, tumor cells plated on 12-well plates were infected with oHSV at MOI=0.2. After oHSV adsorption, media was replaced and culture continued. Twelve, 24, 48 and 72 hours post oHSV infection, culture supernatants were harvested. Titers of infectious oHSV were determined by plaque assay on Vero cells (American Type Culture Collection, Manassas, MA).

Co-cultures of MSC and melanoma cells: MSC or mMSC were freshly infected with oHSV-mCh (MOI=2) for 2 hrs, washed with PBS 3 times and then co-cultured with MeWo-GFP or Y1.1-GFl cells at indicated ratio on 24-well plate ($0.5x10^5$/well; Costar) in MSC culture medium. MeWo cells were then assessed for both the infection of oHSV-mCh and the cell lysis caused by oHSV infection via counting the GFP^+ and $mCherry^+$ cell numbers. Cell viability assay of Y1.1-GFl cells was performed by measuring the *in vitro* Fluc bioluminescence as previously described (1). In parallel, MeWo-GFP-Fluc cells were cultured alone or co-cultured with MSC at 1:1 ratio in a 24-well plate ($0.5x10^5$/well; Costar) in MSC culture medium. Cell viability assay of MeWo cells was performed by measuring the *in vitro* Fluc bioluminescence as described above.

Melanoma brain metastasis mouse models: Mice (6~8 weeks of age, Charles River Laboratories, Wilmington, MA) were anesthetized with ketamine-xylazine and an incision was made to expose the right carotid artery. Using 8-0 sutures, both common and internal carotid arteries were temporally ligated and a catheter connected to a 1ml syringe was inserted into the external carotid artery to inject tumor cells. Two hundred thousand MeWo-FmC or M12-FmC melanoma tumor cells suspended in 100 µl PBS were slowly injected through the catheter. The external artery was then permanently ligated under the dissecting scope (Olympus, SZX10) using fine surgical tools and blood circulation was restored by releasing both common and internal carotid blood flow. Mice were imaged for the success of tumor cell injection 7 days post-implantation and then periodically for tumor progression by *in vivo* BLI. In addition,

the number of metastatic lesions was defined by measuring the number of mCherry-positive foci using ImageJ tools (NIH). Accordingly, each composite image was subjected to ImageJ particle analysis and the number of mCherry-positive particles per section was plotted. Similar procedures were performed to develop syngeneic mouse tumor model using $2x10^5$ Y1.1-GFl in C57BL6 mice. Mice were imaged for tumor cell presence 7 days post-implantation and then periodically for tumor progression by *in vivo* BLI. All *in vivo* procedures were approved by the Subcommittee on Research Animal Care at Massachusetts General Hospital.

Western blot analysis of nectin-1 and cleaved PARP: MeWo, M12, M15 and human MSC cultures were collected and protein lysates were prepared by standard method. Commercial 4~12% Tris-Glycine SDS-Gel were used for all western blots. BMET02 cells were treated with TRAIL for 8 hrs, while MeWo cells were treated with oHSV for 24 or 48 hrs, cell lysates were collected for western blot assay. Nectin-1 antibody was purchased from R&D, cl-PARP and β-actin antibodies are from Cell Signaling.

***In vivo* studies with human melanoma lines:** Female SCID mice (6-8 weeks old) obtained from Charles River laboratories (Wilmington, MA) were used in four different *in vivo* experiments. 1) To track the fate of oHSV delivered by MSC and the dynamics of oHSV spread *in vivo*, MSC were infected with oHSV-Fluc (MOI=2) for 2 hrs, washed with PBS 3 times and 200,000 MSC-oHSV-Fluc cells were intracarotidly injected into either naive mice (without brain tumor, n=3) or brain tumor bearing mice (100,000 MeWo-GFP cells were intracranial implanted into the mice brains 14 days prior to MSC-oHSV-Fluc injection, n=3). The fate of oHSV was assessed by Fluc bioluminescence imaging over time as described previously (2). 2) To directly visualize the distribution of oHSV delivered by MSC in tumor bearing mice, 200,000 MSC cells loaded with oHSV-mCherry (MOI=2) were ICA injected into mice bearing MeWo-GFP or M12-GFP-Fluc brain tumors as described above. oHSV distribution was assessed by fluorescence microscopy on brain sections obtained post MSC-oHSV-mCh injection (48h, 72h and 120h, n=3 mice per time points, 3-5 brain sections from each mice were analyzed). Briefly, mice were sacrificed and brains were dissected as described previously. Fourteen μM sections were assessed for GFP and mCherry representing tumor cells and oHSV, respectively. Higher magnification images

were acquired with Olympus Digital Imaging Software (CellSens). Detailed section analysis was performed using Confocal microscopy (LSM Pascal, Zeiss). 3) To test the therapeutic potential of MSC-oHSV in melanoma brain metastasis, $2x10^5$ MeWo-FmC or M12-FmC cells were ICA injected into SCID mice (surgical manipulation was performed on ECA, and CCA was still intact at this time) and the metastatic tumor growth in the brain was further confirmed by *in vivo* BLI. Two weeks post-tumor cell injection, mice bearing metastatic brain tumors were treated with either MSC or MSC-oHSV via ipsilateral ICA administration and CCA was then permanently closed or ipsilateral ICA injection for the first treatment plus contralateral ICA injection for the second treatment. Mice were then followed for changes in brain tumor volumes by BLI as well as survival analysis. 4) To study the influence of naïve MSC on MeWo tumor growth, mice bearing MeWo-FmC tumors (n=10) were ICA injected with MSC (200,000 cells per mouse, n=5) or PBS (n=5). Mice were then followed for changes in brain tumor volumes by BLI.

***In vivo* studies with mouse melanoma lines:** To test the therapeutic potential of mMSC-oHSV in melanoma brain metastasis, $2x10^5$ Y1.1-GFl were ICA injected into C57BL6 mice and the metastatic tumor growth in the brain was followed by *in vivo* BLI. Two weeks post-tumor cell injection, mice bearing metastatic brain tumors were divided into four groups, untreated control group, mMSC-oHSV treated group (200,000 mMSC-oHSV were ICA injected on d14), anti-PD-L1 treated group (200, 100 and 100 µg anti-PD-L1 antibody (10F9G2) were intraperitoneally (i.p.) injected on d17, d18 and d20 respectively), and mMSC-oHSV plus anti-PD-L1 treated group (mMSC-oHSV were ICA administrated at d14, followed by i.p. injection of anti-PD-L1 at d17, d18 and d20 respectively). Mice were then followed for survival analysis and immunohistochemistry.

Flow cytometric analysis of tumor-infiltrating lymphocytes: To analyze the tumor-infiltrating lymphocyte populations post treatment, C57BL/6 mice were intracranially implanted with YUMM1.1 metastatic brain tumors (d0), two weeks post tumor cells implantation, brain tumor bearing mice were divided into four groups, untreated control group; mMSC-oHSV treated group in which 200,000 mMSC-oHSV cells were ICA administrated in each mouse at d14; anti-PD-L1 treated group in which PD-L1 antibody (10F9G2) were i.p. injected in mice at d17 (200ug/100ul PBS per mouse), d18 (100ug) and d20

(100ug) respectively; and the combination treatment of mMSC-oHSV+anti-PD-L1 group in which mMSC-oHSV were ICA administrated at d14, followed by i.p. injection of anti-PD-L1 at d17, d18 and d20 respectively. At d21, all the mice were sacrificed and brain tumors were harvested, minced with grinder, and digested with DNase I and Collagenase D, followed by Percoll gradient centrifugation to obtain TIL. Next, the samples were resuspended in FACS buffer for staining of mouse CD4-PE and CD8-PE-Cy7 (eBioscience); and intracellular staining was performed for mouse IFNγ-FITC (eBioscience). Samples were run on a BD LSRII Flow Cytometer (BD Biosciences) and data were analyzed using FlowJo Software version 7.6.5 (Tree Star).

References:

1. Bagci-Onder T, Du W, Figueiredo JL, Martinez-Quintanilla J, & Shah K (2015) Targeting breast to brain metastatic tumours with death receptor ligand expressing therapeutic stem cells. *Brain : a journal of neurology* 138(Pt 6):1710-1721.
2. Tamura K*, et al.* (2013) Multimechanistic tumor targeted oncolytic virus overcomes resistance in brain tumors. *Molecular therapy : the journal of the American Society of Gene Therapy* 21(1):68-77.